Author for correspondence:
Ch. Narshimha,
Email: drsimhaou@gmail.com

CAMBRIDGE
UNIVERSITY PRESS

Geochemistry and new zircon U–Pb geochronology of Mesoproterozoic Punugodu granite pluton, SE India: implications for anorogenic magmatism along the western margin of Nellore Schist Belt, India

Ch. Narshimha[1,2] , V. V. Sesha Sai[3], U. V. B. Reddy[2], T. Vijaya Kumar[4],
E. V. S. S. K. Babu[4], B. Sreenivas[4] and K. S. V. Subramanyam[4]

[1]Department of Geology, Center of Advanced Study, Kumaun University, Nainital, 263002, Uttarakhand, India; [2]Department of Applied Geochemistry, Osmania University, Hyderabad-500 007, India; [3]Geological Survey of India, Central Region, Nagpur-440006, India and [4]CSIR – National Geophysical Research Institute, Hyderabad-500007, India

Abstract

We report a new zircon U–Pb age of 1257 ± 6 Ma for the Punugodu granite (PG) pluton in the Eastern Dharwar Craton (EDC), Southern India. The Mesoproterozoic PG is alkali feldspar hypersolvus granite emplaced at shallow crustal level, as evident from the presence of rhyodacite xenoliths and hornfelsic texture developed in the metavolcanic country rocks of the Neoarchaean Nellore Schist Belt (NSB). Geochemically, the PG is metaluminous, ferroan and alkali-calcic, and is characterized by high SiO_2 and $Na_2O + K_2O$, Ga/Al ratios >2.6, high-field-strength elements and rare earth element (REE) contents with low CaO, MgO and Sr, indicating its similarity to anorogenic, alkali (A-type) granite. The highly fractionated REE patterns with negative europium anomalies of PG reflect its evolved nature and feldspar fractionation. Mafic (MME) to hybrid (HME) microgranular enclaves represent distinct batches of mantle-derived magmas that interacted, mingled and undercooled within the partly crystalline PG host magma. Felsic microgranular enclaves (FME) having similar mineralogical and geochemical characteristics to the host PG most likely represent fragments of marginal rock facies of the PG pluton. The PG appears to be formed from an oceanic island basalt (OIB)-like source in an anorogenic, within-plate setting. The emplacement of PG (*c.* 1257 Ma) in the vicinity of Mesoproterozoic Kanigiri Ophiolite (*c.* 1334 Ma) shows an age gap of nearly 77 Ma, which probably suggests PG emplacement in an extensional environment along a terrain boundary at the western margin of the Neoarchaean NSB in the EDC.

1. Introduction

Globally, A-type granites occur in Precambrian and Phanerozoic terrains, mainly in extensional tectonic settings (e.g. Loiselle & Wones, 1979; Eby, 1990, 1992; Black & Liégeois, 1993). A-type granites are distinct from other granite types and are defined as relatively anhydrous with high SiO_2, high $Na_2O + K_2O$, low MgO and high incompatible trace element contents including REE, Zr, Y, Nb and Ta (e.g. Eby, 1992; Frost *et al.* 1999; Bonin, 2007; Dall'Agnol *et al.* 2012; Li *et al.* 2014). A-type granites predominantly range from single-feldspar (hypersolvus) to two-feldspar (subsolvus) granites. In the hypersolvus varieties, the granitic rocks are composed of quartz and alkali feldspar; the latter yields coarse perthitic exsolution (e.g. Turner *et al.* 1992).

Several mechanisms have been proposed to explain the origin of A-type magmas: (1) direct fractionation of mantle-derived alkaline basalts (e.g. Turner *et al.* 1992; Litvinovsky *et al.* 2002; Mushkin *et al.* 2003); (2) low degrees of partial melting of F^-- and Cl^--enriched dry, lower-crustal granulitic residue from which a granite melt was previously extracted (e.g. Collins *et al.* 1982; Clemens *et al.* 1986; King *et al.* 1997); (3) low-pressure melting of calc-alkaline rocks at upper crustal levels (Skjerlie & Johnston, 1993; Patiño Douce, 1997); and (4) hybridization between anatectic granitic and mantle-derived mafic magmas (Bedard, 1990; Kerr & Fryer, 1993; Wickham *et al.* 1996; Mingram *et al.* 2000).

Although fine-grained, dark-coloured microgranular enclaves are most common in calc-alkaline, metaluminous (I-type) granites (e.g. Didier & Barbarin, 1991; Kumar and Rino, 2006), they also occur in A-type granites and provide vital clues on the processes that have acted at different levels during the magma evolutionary history (Bonin, 1991). Further, microgranular enclaves and their distribution in felsic plutons, along with their textural and contact

relationships with felsic host, may provide insights into the magma chamber processes and dynamics (e.g. Vernon, 1984; Vernon et al. 1988; Kumar, 1995, 2010, 2020; Perugini et al. 2007).

In Peninsular India, A-type granites are widely distributed along the marginal zone of the Eastern Ghat Granulite Belt (EGGB), in the Southern Granulite Terrain, Mahakoshal Supracrustal Belt, Central India; the Mayurbhanj area, north of the Bastar Craton; and the Malani Igneous Province (e.g. Eby & Kochhar, 1990; Meert et al. 2010; Sarvothman & Sesha Sai, 2010; Kumar et al. 2020; Yadav et al. 2020). In Southern India, the western margin of the Neoarchaean Nellore Schist Belt (NSB) is characterized by the emplacement of several granite plutons of Proterozoic age (Gupta et al. 1984; Dobmeier et al. 2006; Sesha Sai, 2013). These granite plutons form part of the Proterozoic granite emplacement zone located close to a major terrain boundary in the Eastern Dharwar Craton (EDC), i.e. the eastern margin of the Proterozoic Cuddapah Basin and Neoarchaean NSB. The Punugodu granite (PG) is one among these granite plutons spatially associated with other granites, gabbros, felsic volcanics and ophiolite mélange rocks. The origin and evolution of PG have not yet been described. The present study therefore aimed to carry out a detailed investigation involving the field relation, petrography, geochemistry and geochronology of the PG occurring to the east of Cuddapah Basin, in order to characterize and discuss its petrogenesis, which may contribute to our understanding of the Proterozoic accretionary and rifting history of this region.

2. Geological setting

The Neoarchaean NSB constituted by metavolcanics and metasediments is characterized by emplacement of mafic and felsic magmatic rocks of Proterozoic age (e.g. Vasudevan & Rao, 1976; Gupta et al. 1984; Srinivasan & Roop Kumar, 1995; Raman & Murty, 1997; Dharma Rao & Reddy, 2007; Ravikant, 2010; Sesha Sai et al. 2013; Saha et al. 2015). The two domains that constitute the NSB are the upper western Udaigiri and the lower eastern Vinjamuru domains (Dobmeier & Raith, 2003; Saha et al. 2015). The mafic and felsic alkaline plutons of the NSB fall within the southern continuity of the Prakasam Alkaline Province (PAkP) (Ratnakar & Leelanandam 1985; Rao et al. 1988; Ratnakar & Vijaya Kumar, 1995; Leelanandam et al. 2006). Several collision- and extension-related Proterozoic magmatic events played a significant role in the crustal accretion and growth to the east of Cuddapah Basin in the EDC (Divakara Rao et al. 1999; French et al. 2008; Dharma Rao et al. 2011; Sain et al. 2017; Sesha Sai, 2019).

The occurrence of ophiolite affinity rocks at Kandra (Kandra Ophiolite Complex) in the southern part of the NSB indicates that subduction would have initiated ~1.85 Ga (Sesha Sai, 2009; Vijaya Kumar et al. 2010). The eastern margin of the EDC evolved as the site for collision with the Napier Complex forming the 1.7–1.55 Ga old orogen (Chaudhuri et al. 2002; Dobmeier & Raith, 2003; Ravikant 2010; Vijaya Kumar et al. 2010), resulting in the formation of granulites (1700 Ma), anorthosite (1690–1630 Ma) and granites (1650–1450 Ma) in the Ongole domain (Kovach et al. 2001; Simmat & Raith, 2008; Dharma Rao et al. 2012). The overlapping ages of these rocks indicates that the domain was magmatically active between at least c. 1720 and 1570 Ma (Henderson et al. 2014).

The plutons emplaced in the northern part of the NSB in the PAkP yield the zircon U–Pb Mesoproterozoic ages of Elchuru nepheline syenite (1321 ± 17 Ma; Upadhyay et al. 2006),

Purimetla gabbro (1334 ± 15 Ma; Subramanyam et al. 2016), Uppalapadu nepheline syenite (1356 ± 41 Ma; Vijaya Kumar et al. 2007), Errakonda ferrosyenite (1352 ± 2 Ma; Vijaya Kumar et al. 2007) and Kanigiri gabbro (1338 ± 27 Ma; Subramanyam et al. 2016), which are emplaced between the Udaigiri and Vinjamuru domains. The Kanigiri granite (1284 ± 4 Ma; Sain et al. 2017), Punugodu granite (PG) (1256 ± 6 Ma; present study) and Peddacharlopalle gabbro (1251.2 ± 9.4 Ma; Subramanyam et al. 2016) are ~100 Ma younger than the PAk rocks. The 1334 ± 20 Ma age of Kanigiri Ophiolite Mélange and the age of the plutons emplaced in its vicinity show a gap of ~80 Ma. However, further studies are required on those undated southern and northern plutons of the NSB and PAkP to shed light on the tectono-magmatic evolution of the NSB.

3. Field relationships and petrography

The PG pluton, covering an area of 7 km^2, occurs as a N–S-trending oval-shaped body commonly exposed to the east of Kanigiri granite and south of the Podili granite plutons (Fig. 1). Xenoliths of the pre-existing NSB volcanics are found hosted in the PG. These xenoliths are felsic, angular and fractured, and show sharp to partly reactive contacts with the host PG (Fig. 2a). In places, calc-silicate bands (Fig. 2b) of the pre-existing NSB are also observed. Reddy & Sesha Sai (2003) reported a rhyodacitic (metavolcanic) rock having intimate contact with the PG. Along the contact with PG the hornfelsic textures are developed (Fig. 2c), which clearly indicate intrusive contact formed by thermal metamorphism. Therefore, the rhyodacite represents pre-existing supracrustal NSB rock, now engulfed into the PG, and formed the large xenolith. In the southern margin of PG, contact with the chlorite schist of NSB is observed (Fig. 2d). Due to soil development and the weathered contact of PG and chlorite schist of NSB, the actual nature of the contact is unknown.

The PG hosts abundant microgranular enclaves (ME). These ME are fine-grained, mafic–melanocratic (MME) to porphyritic (hybrid) mesocratic (HME), and vary in size from a few mm to metres, with rounded, elliptical, spherical and lenticular shapes commonly having sharp, crenulated and occasionally diffuse contacts with the host PG (Fig. 2e–h). These field features of ME indicate ME magma mingling and undercooling within the partly crystalline PG melt (e.g. Kumar et al. 2004). The HME exhibit characteristics that are intermediate between MME and felsic microgranular enclaves (FME) (Fig. 2f). The N–S-oriented nature of ME perhaps indicates the phenomenon of magmatic flowage attained during the emplacement and dynamics of coexisting ME and PG magmas (Fig. 2g) prior to solidification of the entire system as described by Kumar (2020). The FME are fine-grained, linear to spherical to lenticular (Fig. 2h), most likely representing fragments of early, chilled margin facies of PG pluton and disrupted as FME due to prevailing convective force in the PG chamber (e.g. Didier & Barbarin, 1991; Kumar, 2010). The depth of emplacement is one factor that plays a vital role in the crystallization of A-type alkali feldspar granites. Felsic magmas of A-type affinity are products of residual liquids resulting from the differentiation phenomenon in the magma chambers with varying depths (Bonin, 1998).

A total of 29 rock samples, comprising 14 PG, four xenoliths, four FME, three HME and four MME samples, were collected during fieldwork covering the outcrops of PG pluton. Sample locations are shown in Figure 1.
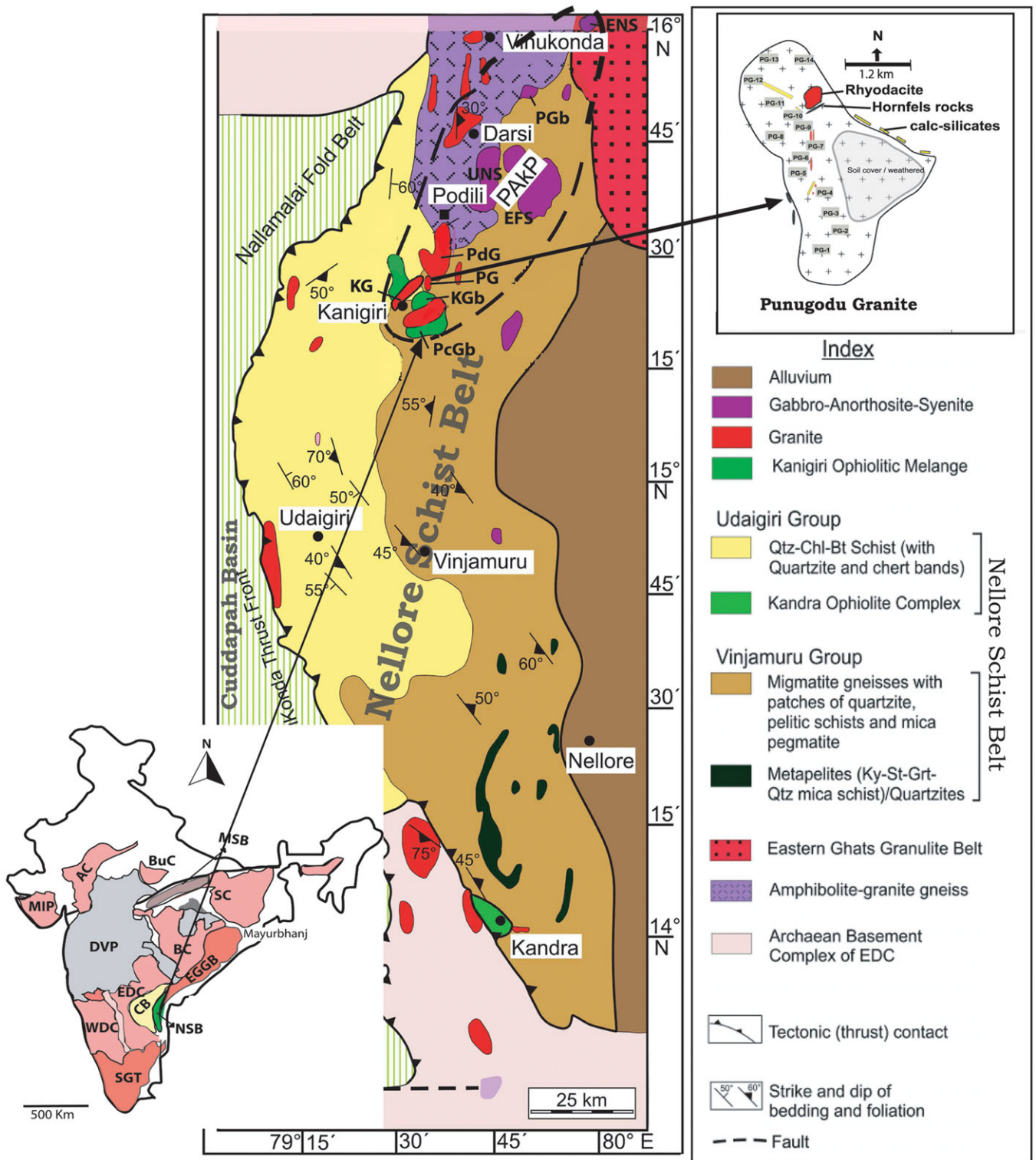
Fig. 1. (Colour online) Geological map of Nellore Schist Belt and Prakasam Alkaline Province, after Srinivasan & Roop Kumar (1995) and Sesha Sai (2013). Map of Punugodu granite pluton is given in the inset. NSB: Nellore Schist Belt; PAkP: Prakasam Alkaline Province; ENS: Elchuru nepheline syenite; PGb: Purimetla gabbro; UNS: Uppalapadu nepheline syenite; EFS: Errakonda ferosyenite; PdG: Podili granite; PG: Punugodu granite; KGb: Kanigiri gabbro; KG: Kanigiri granite; PcGb: Peddacharlapalle gabbro; AC: Aravali Craton; MIP: Malani Igneous Province; BuC: Bundelkhand Craton; SC: Singhbhum Craton; BC: Bastar Craton; DVP: Deccan Volcanic Province; EGGB: Eastern Ghats Granulite Belt; CB: Cuddapah Basin; WDC: Western Dharwar Craton; EDC: Eastern Dharwar Craton; SGT: Southern Granulite Terrain; MSB: Mahakoshal Supracrustal Belt.

3.a Petrography of PG

Detailed petrographic studies reveal that the PG is essentially composed of relatively large subhedral laths of perthitic K-feldspar and quartz, while the mafic phases noticed are biotite and amphibole, with zircon, titanite, fluorite, apatite and opaques as the accessories. Relict clinopyroxene is also noticed in places in
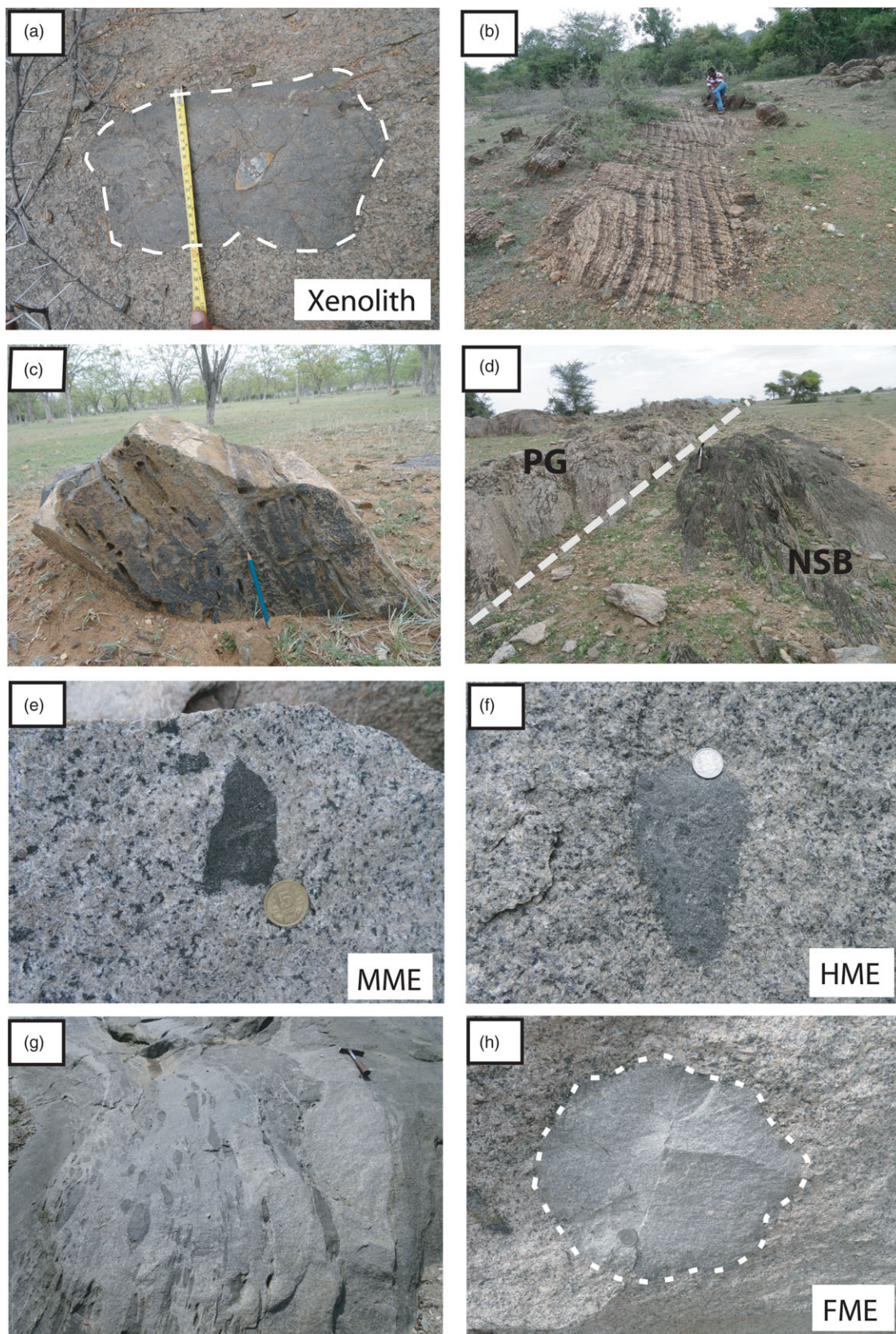
Fig. 2. (Colour online) Field photographs showing the field relationship of the PG pluton. (a) Xenolith with fractures showing sharp contact with host rock. (b) Occurrence of a calc-silicate xenolith of NSB in PG. (c) Presence of hornfelsic rock at the contact with pre-existing metavolcanic rock. (d) Field photograph showing contact between PG and chlorite schist of NSB country rock. (e) Fine-grained, mafic microgranular enclave surrounded by mafic clusters. (f) Hybrid microgranular enclave with ellipsoidal shape. (g) Field photograph showing oriented nature of Mesgmatic enclaves at the pluton contact indicating magma mingling. (h) Fine-grained felsic microgranular enclave with rounded shape.

the PG. Amphibole is pleochroic in shades of brown to blue. The presence of single feldspar in the form of microcline perthite indicates the hypersolvus nature of PG (Fig. 3a and b). Petrographic studies of the PG samples collected along the margins of the pluton reveal that quartz is anhedral and exhibits wavy extinction and recrystallization indicating a deformational regime (Fig. 3c). Perthitic K-feldspars are characteristically twinned (Fig. 3d). Perthite occurs as string, vein and patchy types (Anderson, 1928; Smithson, 1963). String perthites are formed due to exsolution, as evident from small, well-oriented blebs perthites, whereas the patchy and coarse vein types of perthites are formed due to replacement evident from irregular, redistributed and enlarged albite blebs, which occur close to and on the margin of the grain (e.g. Alling, 1938). Fluorite is observed, associated with biotite (Fig. 3e). Bluish amphibole occurs as subhedral prismatic grains in places (Fig. 3f). Clusters of mafic phases represented mainly by amphiboles and associated opaques are observed in parts of the quartzo-feldspathic material (Fig. 3g). Fine-grained skeletal opaques are observed in the vicinity of biotite and amphibole. Zircon is euhedral and exhibits zoning (Fig. 3h).

3.b. Petrography of enclaves

Petrographic studies indicated variation in the mineralogy of three types of magmatic enclaves observed in PG, namely FME, HME and MME. The FMEs are mineralogically similar to host granite and mainly consist of quartz, microcline, plagioclase and biotite (Fig. 4a and b). The HMEs are fine-grained and porphyritic, exhibiting typical igneous texture with felsic phenocrysts (xenocrysts). Quartz xenocrysts (ocelli) with biotite and hornblende-rich mantle (Fig. 4c), perthites and opaques with biotite rim and clusters are common (Fig. 4d). Mineralogically, the MMEs consist of plagioclase and pyroxene as essential minerals and exhibit subophitic texture (Fig. 4e). Twinned plagioclase crystals occur as elongated laths in places in the MMEs, a textural feature suggesting magmatic origin (Fig. 4 f). Biotite appears as interstitial flakes in the MMEs. Subhedral grains of Fe-oxides occur as accessory minerals in the MMEs (Fig. 4g). Most MMEs show diffusive and cuspate contacts with host PG, indicating their magmatic nature. This type of enclave contact mainly appears in some particular cases where large volumes of mafic magma dominate over felsic magma (Barbarin & Didier, 1991). The enclaves as xenoliths represent the caught-up patches of the NSB metavolcanics and hence are different from the observed ME types. Xenoliths show feeble deformation, which is evident from the recrystallized quartz and distorted twin lamellae in plagioclase. Petrographic studies show the presence in the metavolcanic xenolith of quartz porphyroclasts along with feldspar, hornblende and biotite (Fig. 4h).

4. Sampling and analytical techniques

Relatively fresh and unweathered samples were collected during the fieldwork. High-quality thin-sections were made for the systematic petrographic studies. Rock samples for major, trace and rare earth elemental analysis were crushed and pulverized to fine powders manually using the agate mortar and pestle.

4.a. Major oxides and trace elements

Geochemical analyses were carried out at the Geochemistry Division, CSIR – National Geophysical Research Institute (NGRI), Hyderabad, India. Major-element abundances were determined on pressed powder pellets using X-Ray Fluorescence (XRF)

(Phillips MAGIX PRO Model 2440) following the methods outlined by Krishna *et al.* (2007). Trace and rare earth elements were determined by high-resolution inductively coupled mass spectrometer (HR-ICP-MS; Nu Instruments Attom, UK) in jump wiggle mode. The analytical procedure, precision and accuracy for HR-ICP-MS are reported in Manikyamba *et al.* (2016). [103]Rh was used as an internal standard, and external drift was corrected by repeated analyses of standards used for calibration.

4.b. Zircon separation and U–Pb analysis

Zircon grain extractions were carried out after crushing the rock samples into ~80–250 μm sieve fractions and were processed on the Wilfley shake table to separate heavy mineral fractions. The heavies were then subjected to isodynamic magnetic separation before handpicking zircons under a binocular microscope. Zircon grains were mounted in 25 mm epoxy resin blocks, diamond-polished, carbon-coated and cathodoluminescence (CL)-imaged on a TESCAN LM3H SEM mounted with a Rainbow colour CL detector. Zircon U–Pb dating was performed using Thermo X Series[II] ICP-MS coupled to a New Wave Universal Platform 213 nm Nd–YAG laser ablation system with a large-format ablation cell operated with a combination of He and Ar gases as detailed in Babu *et al.* (2009). The data were processed offline using 'IsoplotR' (Vermeesh, 2018) and 'Glitter software' to compute the ages and corrected for common Pb using Andersen's scheme (Andersen, 2002).

Results

The major, trace and rare earth element data of the granite samples, along with those of the xenoliths, FME, HME and MME analysed in the present study, are presented in Table 1.

5.a. Geochemistry of PG and enclaves

Major-oxide geochemistry of PG reveals high SiO_2 (avg. 70.41 wt %) and high $Na_2O + K_2O$ (avg, 9.40 wt %) contents, a feature that corresponds to the anorogenic, alkali (A-type) granites (Whalen *et al.* 1987). The SiO_2 concentrations in enclaves are as follows: in xenoliths from 61.2 to 64.9 wt %, FME from 66.5 to 67.4 wt %, HME from 49.4 to 62.9 wt % and MME from 45.2 to 49 wt %. The $K_2O + Na_2O$ content in xenoliths, FME, HME and MME ranges from 8.58 to 9.48 wt %, 8.27 to 9.5 wt %, 8.34 to 9.25 wt % and 3.74 to 5.24 wt % respectively. A detailed account of major oxide, trace element and rare earth element geochemical characteristics of PG pluton was presented previously (Narshimha *et al.* 2018). In the MALI ($Na_2O + K_2O$–CaO) vs silica diagram (Frost *et al.* 2001), the PG granite, FME and xenoliths exhibit an alkaline to alkali-calcic trend (Fig. 5a). The MMEs in the FeO* vs silica diagram (Frost & Frost, 2008) occupy the tholeiitic and alkaline fields (Fig. 5b). The Fe number of 13 PG samples varies from 0.76 to 0.97, indicating its strong ferron character. In the A/NK–A/CNK alumina saturation diagram (Fig. 5c), the majority of PG samples fall in the metaluminous domain, while a few fall close to the boundary of the metaluminous and peralkaline fields (Shand, 1943). In the normative anorthite (An) – albite (Ab) – orthoclase (Or) diagram (O'Connor, 1965), the samples fall in the granite field (Fig. 5d). In the R_1–R_2 multicationic parameters (De la Roche *et al.* 1980)-based tectonic classification scheme (after Batchelor & Bowden, 1985), the PG shows affinity with syn-collision to late orogenic tectonic settings (Fig. 5e). Pearce *et al.* (1984) classified the granites into a within-plate, collisional,
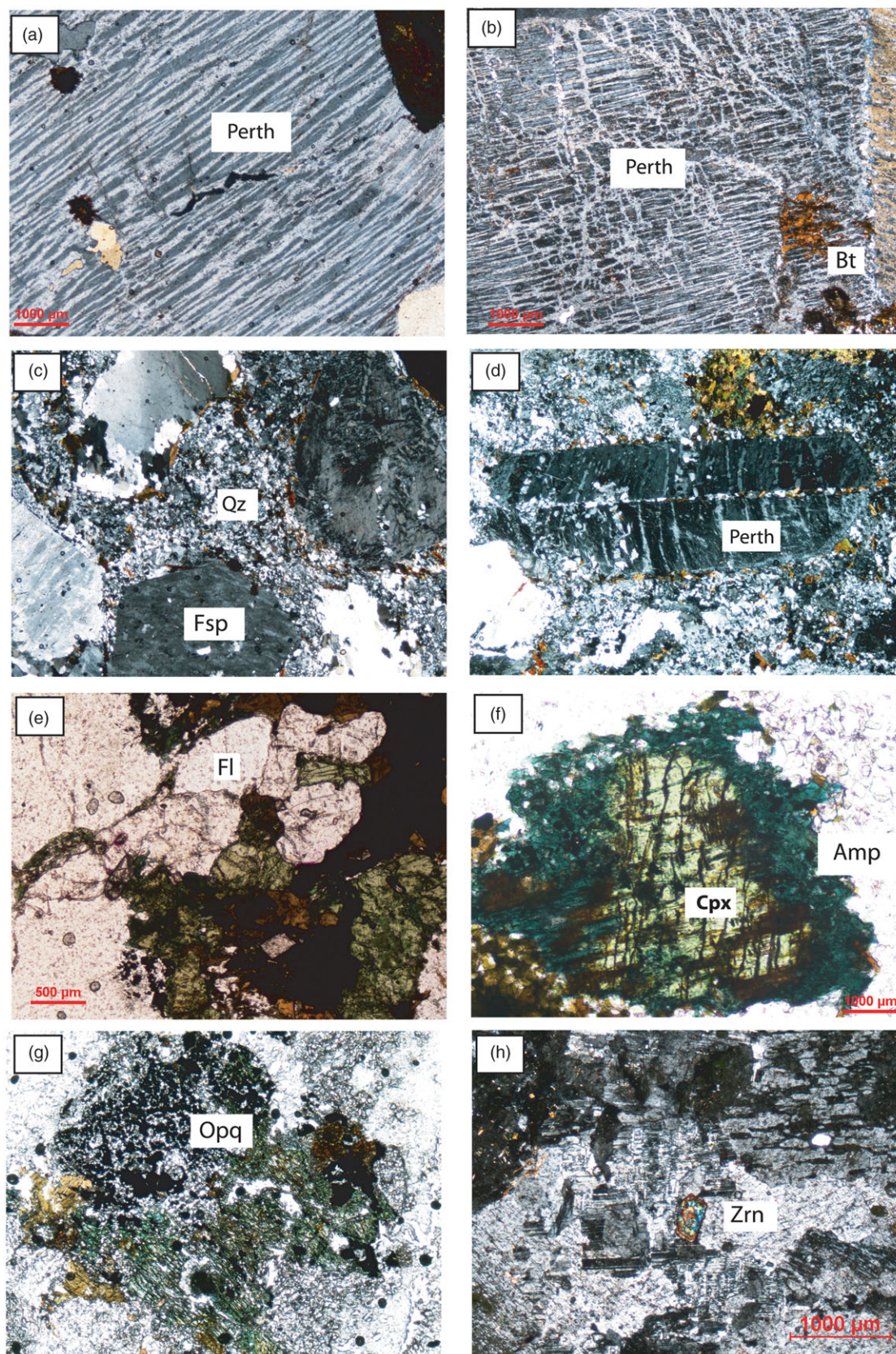
Fig. 3. (Colour online) (a) Photomicrograph under crossed Nicols showing coarse-grained perthitic feldspar. (b) Photomicrograph of microcline microperthite with biotite cluster. (c) Admixture of recrystallized quartz along with the feldspar grain boundary indicating recrystallization due to deformation. (d) Photomicrograph under crossed Nicols showing Carlsbad twinning in perthitic K-feldspar. (e) Photomicrograph in plane-polarized light showing fluorite associated with biotite. (f) Photomicrograph in plane-polarized light showing relict clinopyroxene surrounded by alkali amphibole. (g) Photomicrograph in plane-polarized light showing skeletal opaques in the vicinity of mafic minerals. (h) Zoned euhedral zircon (plane polarized light). Mineral abbreviations used as in Whitney & Evans (2010).
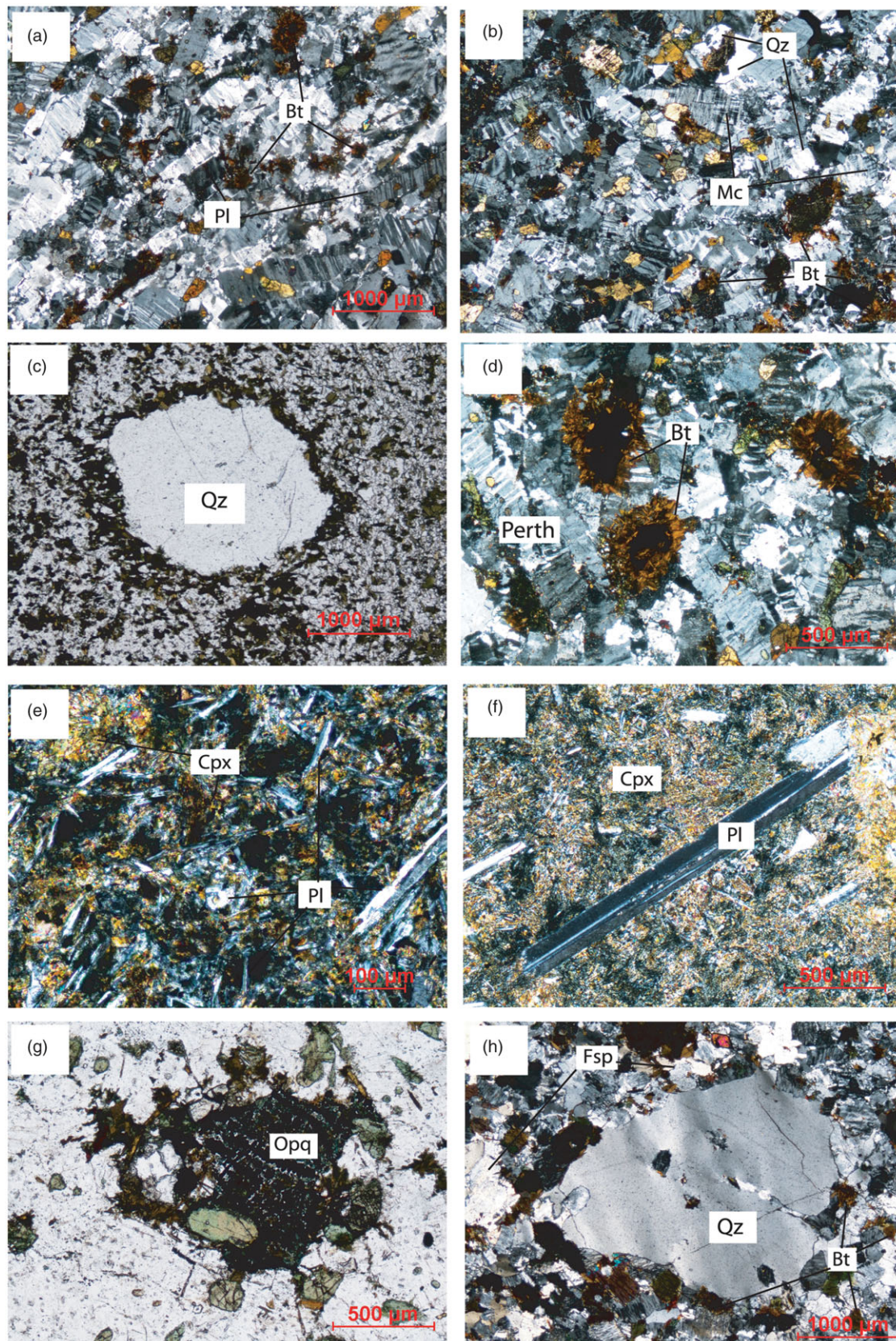
Fig. 4. (Colour online) (a, b) Photomicrographs under crossed Nicols showing quartz, plagioclase, microcline and biotite minerals in FME (c) Photomicrograph under plain polarized light showing quartz xenocrysts with biotite- and hornblende-rich mantle in HME. (d) Photomicrographs under crossed Nicols showing perthites and clusters of biotite in HME. (e, f) Photomicrograph showing plagioclase and pyroxene with sub-ophitic texture in MME. (g) Photomicrograph showing the cluster of opaques in MME. (h) Photomicrograph under crossed Nicols showing quartz porphyroclast in NSB metavolcanic xenolith.

Table 1. Major oxide analysis (%), trace and rare earth element analyses (ppm) of Punugodu granite pluton and enclaves

Sl. No.	1	2	3	4	5	6	7	8	9	10	11	12	13	14
Granite														
Sample	PG-1	PG-2	PG-3	PG4	PG-5	PG-6	PG-7	PG-8	PG-9	PG-10	PG-11	PG-12	PG-13	PG-14
Major elements (wt %)														
SiO_2	71.2	64.9	71.2	69.8	71.4	69.6	72.7	69.5	68.9	70.2	73.1	71.8	71.3	70.2
Al_2O_3	13.3	13.9	12.5	13.2	13.4	13.3	11.7	14.5	13.8	13.3	12.0	13.7	13.7	14.2
Fe_2O_3	3.6	4.6	2.9	3.6	3.2	3.4	3.0	3.0	3.6	3.0	3.2	2.3	2.7	2.9
MnO	0.1	0.1	0.1	0.1	0.1	0.1	0.1	0.1	0.1	0.1	0.1	0.0	0.1	0.1
MgO	0.1	3.6	1.1	0.5	0.3	0.8	0.6	0.2	0.9	0.6	0.3	0.3	0.2	0.9
CaO	1.0	3.1	1.2	1.2	1.0	0.9	1.0	0.9	1.3	1.1	0.7	1.0	0.8	1.1
Na_2O	3.3	4.0	3.5	3.7	3.4	3.7	3.6	3.8	3.5	3.3	3.6	3.4	3.8	3.6
K_2O	6.0	3.8	5.9	6.3	5.8	6.4	5.7	6.4	5.6	6.4	5.7	5.7	6.2	5.7
TiO_2	0.4	0.5	0.3	0.4	0.3	0.3	0.3	0.3	0.3	0.3	0.3	0.2	0.3	0.3
P_2O_5	0.0	0.1	0.1	0.0	0.0	0.0	0.0	0.0	0.1	0.0	0.0	0.0	0.0	0.0
LOI	0.6	1.1	0.7	0.8	0.5	0.7	0.5	1.2	0.8	1.1	0.6	0.8	0.8	0.3
SUM	99.6	99.7	99.4	99.4	99.4	99.2	99.1	99.8	98.8	99.4	99.4	99.2	99.7	99.1
Fe#.	0.97	0.56	0.72	0.87	0.91	0.81	0.83	0.93	0.80	0.83	0.88	0.88	0.93	0.76
Trace elements (ppm)														
La	312.8	101.4	242.5	320.0	187.9	161.3	144.1	160.5	191.3	179.2	170.0	215.0	225.7	170.9
Ce	1056.7	190.2	469.8	1047.8	360.0	314.8	280.4	314.3	373.7	336.1	326.9	427.4	439.4	332.3
Pr	64.9	19.2	49.9	62.2	36.8	32.9	29.2	33.2	39.3	34.6	35.1	43.5	46.0	34.5
Nd	238.7	69.4	184.6	224.2	133.3	119.4	105.8	120.9	144.0	125.5	129.7	149.9	167.2	124.8
Sm	46.3	13.1	35.5	39.4	25.7	24.0	21.6	24.0	28.5	23.7	26.8	27.7	32.5	24.7
Eu	0.5	0.8	0.5	0.6	0.5	0.5	0.4	0.5	0.6	0.5	0.6	0.5	0.4	0.5
Gd	38.3	11.4	29.2	32.1	22.1	20.7	18.8	20.4	24.5	21.2	23.5	24.7	27.6	21.7
Tb	5.7	1.9	4.3	4.6	3.6	3.5	3.2	3.4	4.0	3.4	4.0	4.4	4.4	3.7
Dy	34.8	13.5	25.2	27.4	24.4	23.9	21.7	22.5	26.2	22.4	27.7	32.0	29.1	24.8
Ho	3.6	1.6	2.6	2.8	2.8	2.8	2.5	2.5	2.9	2.6	3.2	3.9	3.2	2.8
Er	11.2	5.5	7.7	9.2	9.0	9.0	8.2	8.4	9.4	8.3	10.2	13.2	10.6	9.2
Tm	1.3	0.7	0.9	1.1	1.1	1.2	1.0	1.0	1.1	1.0	1.3	1.7	1.3	1.2
Yb	12.6	7.7	8.5	11.1	10.8	11.3	10.0	10.1	11.1	10.1	11.8	15.8	12.8	11.2
Lu	2.0	1.3	1.4	1.8	1.7	1.8	1.5	1.6	1.8	1.6	1.9	2.3	2.0	1.7
Sc	1.8	4.7	1.8	1.9	1.9	1.9	1.9	2.0	2.1	2.3	2.0	2.2	2.4	2.1

Table 1. (*Continued*)

Sl. No.	1	2	3	4	5	6	7	8	9	10	11	12	13	14	
Granite															
Sample	PG-1	PG-2	PG-3	PG4	PG-5	PG-6	PG-7	PG-8	PG-9	PG-10	PG-11	PG-12	PG-13	PG-14	
V	2.0	7.9	1.4	1.6	1.3	1.3	1.2	1.2	1.1	1.6	1.1	1.4	1.2	1.4	
Cr	7.9	8.2	7.9	8.1	8.2	8.1	8.3	8.1	8.1	8.1	8.0	8.3	8.0	8.3	
Co	0.4	8.8	0.4	0.4	0.5	0.5	0.6	0.5	0.6	1.2	0.8	1.0	0.5	0.8	
Ni	1.5	4.1	1.4	1.3	1.2	1.2	1.4	1.2	1.4	1.5	1.7	1.3	1.2	1.5	
Cu	0.5	0.7	0.5	0.5	0.5	0.5	0.4	0.5	0.5	0.5	0.5	0.4	0.5	0.5	
Zn	42.3	27.6	37.6	48.9	45.1	52.4	38.8	44.7	44.5	38.4	44.0	21.0	30.2	45.8	
Ga	37.6	26.9	37.0	38.9	36.9	40.4	35.4	40.1	38.3	33.9	36.0	36.0	37.6	38.1	
Rb	197.3	136.4	179.1	224.7	241.2	251.5	225.3	247.3	241.0	212.8	230.6	345.2	278.6	223.2	
Sr	9.6	93.6	10.8	10.4	11.4	9.9	8.4	13.0	12.6	17.8	12.3	15.0	10.7	14.3	
Y	156.6	79.6	108.1	129.5	137.9	137.5	123.6	125.6	141.8	129.0	151.0	201.8	144.7	141.5	
Zr	128.4	341.8	85.5	153.6	279.0	311.8	275.6	274.4	282.0	255.8	296.2	265.4	113.7	356.1	
Nb	216.6	99.3	131.6	194.9	183.0	188.1	167.1	163.0	173.1	184.9	165.7	211.4	190.1	180.0	
Cs	1.6	1.9	1.5	2.0	1.9	2.0	1.6	1.8	2.4	1.6	2.7	2.6	2.6	3.1	
Ba	32.7	243.5	40.0	37.4	58.4	56.4	69.5	69.9	72.5	132.3	131.9	96.9	45.2	89.3	
Hf	4.9	11.8	3.2	6.1	10.2	12.9	10.1	10.2	10.3	8.2	11.3	11.9	4.6	12.7	
Ta	8.2	7.4	4.7	8.2	8.1	11.3	8.5	8.1	8.0	8.5	8.1	12.1	9.0	9.0	
Pb	17.4	23.6	16.9	17.3	21.5	19.8	14.5	19.6	14.8	35.7	17.9	16.0	18.4	16.6	
Th	51.6	35.1	36.4	47.1	43.0	45.0	39.2	38.7	40.4	41.0	41.9	118.4	55.5	44.5	
U	6.0	10.4	3.8	5.2	6.4	6.4	8.4	6.2	5.9	5.0	4.2	20.6	8.0	8.0	
Sl. no.	15	16	17	18	19	20	21	22	23	24	25	26	27	28	29
Enclave															
Sample	Xenolith-1	Xenolith-2	Xenolith-3	Xenolith-4	HME-1	HME-2	HME-3	FME-1	FME-2	FME-3	FME-4	MME-1	MME-2	MME-3	MME-4
Major elements (wt %)															
SiO_2	64.9	64.2	61.5	61.2	53.3	49.4	62.9	66.5	67.4	66.9	66.9	45.2	48.7	49.0	47.6
Al_2O_3	13.2	13.5	13.2	13.1	14.5	11.0	13.8	13.7	13.6	14.0	13.9	13.9	13.1	13.2	13.4
Fe_2O_3	6.4	6.1	7.3	7.9	8.2	10.7	6.7	6.8	6.1	4.3	5.3	11.0	12.0	11.5	11.5
MnO	0.1	0.1	0.1	0.1	0.1	0.2	0.1	0.1	0.1	0.1	0.1	0.1	0.2	0.1	0.1
MgO	0.8	1.3	2.9	3.5	2.9	9.9	0.9	0.4	0.2	0.5	0.5	12.3	7.6	8.2	9.4
CaO	3.1	3.5	3.6	3.5	1.6	6.7	4.0	2.0	1.7	2.7	2.0	9.6	9.7	10.8	10.0

(*Continued*)

Table 1. (*Continued*)

Na_2O	6.0	5.4	6.1	5.1	5.1	4.0	5.8	4.1	4.1	4.8	5.9	2.6	3.7	2.3	2.9
K_2O	3.5	3.7	3.4	3.5	3.2	4.9	3.4	4.2	4.3	4.3	3.6	2.2	1.6	1.4	1.7
TiO_2	0.8	0.7	0.9	1.0	0.5	1.0	0.7	0.7	0.7	0.5	0.5	1.5	1.5	1.8	1.6
P_2O_5	0.1	0.1	0.1	0.1	0.1	0.2	0.1	0.1	0.1	0.1	0.1	0.2	0.2	0.3	0.2
SUM	98.9	98.5	99.2	99.1	89.4	98.1	98.4	98.3	98.2	98.0	98.8	98.6	98.2	98.7	98.5
Trace elements (ppm)															
La	135.4	172.9	149.9	122.3	422.3	121.1	160.1	591.6	598.7	220.0	212.3	71.7	30.4	26.5	42.9
Ce	287.6	316.4	266.4	249.1	821.6	230.7	295.1	1220	1222	386.8	455.9	140.6	63.3	61.4	88.4
Pr	24.6	42.2	29.5	21.0	105.5	30.2	40.9	100.6	101.3	53.7	38.2	18.7	8.9	5.3	11.0
Nd	109.3	132.8	135.2	90.5	409.7	121.2	129.2	426.6	427.0	168.6	166.2	79.1	31.8	26.4	45.7
Sm	21.9	25.9	27.9	18.1	77.9	26.4	26.7	67.8	67.4	31.8	31.0	15.6	7.3	5.4	9.4
Eu	0.8	0.7	1.2	0.8	0.7	0.8	0.6	1.2	1.2	1.0	0.7	1.6	1.5	1.7	1.6
Gd	21.4	20.1	27.0	18.1	76.4	28.8	21.6	66.4	68.1	27.4	31.6	15.2	5.8	5.3	8.8
Tb	3.3	3.6	4.0	2.8	12.7	5.2	3.9	7.8	7.4	4.7	4.3	2.5	1.1	0.8	1.5
Dy	18.0	18.0	19.9	14.7	55.0	24.3	20.3	35.1	32.2	24.2	21.5	11.3	5.8	4.4	7.2
Ho	2.8	3.2	3.0	2.3	10.4	4.9	3.6	5.1	4.6	4.4	3.3	2.2	1.0	0.7	1.3
Er	8.5	9.6	8.4	6.8	35.0	16.8	10.5	14.4	12.9	13.2	9.4	7.6	3.1	2.1	4.3
Tm	1.7	1.4	1.5	1.3	4.3	2.1	1.5	2.6	2.3	1.9	1.8	0.9	0.5	0.4	0.6
Yb	12.1	9.9	10.3	9.5	27.1	13.2	10.6	18.0	16.8	13.1	12.4	5.9	3.3	2.9	4.0
Lu	1.8	1.5	1.4	1.3	4.1	2.0	1.6	2.7	2.6	2.1	1.8	0.9	0.5	0.4	0.6
Sc	9.5	7.3	12.7	14.3	10.4	36.4	7.6	4.3	4.5	6.9	4.7	46.2	31.6	30.2	36.0
V	25.1	39.0	81.9	82.8	41.3	605.1	37.4	5.9	4.9	19.8	25.5	721.9	260.3	215.4	399.2
Cr	164.1	97.3	252.9	176.7	53.3	61.7	113.4	195.9	165.7	99.5	248.9	63.0	74.4	283.8	140.4
Co	5.2	6.2	17.2	18.7	3.6	69.6	5.3	3.2	2.4	4.5	4.7	116.0	37.9	45.4	66.4
Ni	39.8	9.0	51.9	45.8	7.2	44.6	9.5	49.7	43.1	10.4	50.1	88.0	10.6	70.4	56.3
Cu	23.9	3.0	23.9	29.5	62.9	96.4	1.2	21.0	22.3	2.3	39.5	251.6	5.3	42.7	99.8
Zn	173.6	103.6	186.9	196.7	328.6	975.5	95.4	136.4	128.3	116.7	212.1	190.4	73.4	111.8	125.2
Ga	39.8	50.8	42.0	38.3	39.4	26.3	48.1	79.7	79.5	50.1	48.8	22.5	25.0	19.5	22.3
Rb	300.1	319.0	182.9	454.4	290.8	1014	320.1	313.0	270.0	198.7	139.8	111.4	68.4	58.7	79.5
Sr	28.9	28.6	57.4	51.5	13.0	34.0	33.3	34.2	36.8	45.7	56.8	262.1	241.3	385.4	296.3
Y	125.5	127.2	112.1	102.2	366.1	196.3	133.0	187.9	172.4	164.3	134.0	79.9	38.4	28.8	49.0
Zr	596.1	862.3	413.2	397.0	998.5	408.5	606.1	443.9	621.5	722.1	359.4	466.8	263.8	144.4	291.7

(*Continued*)

Table 1. (*Continued*)

Sl. No.	1	2	3	4	5	6	7	8	9	10	11	12	13	14	
Granite															
Sample	PG-1	PG-2	PG-3	PG4	PG-5	PG-6	PG-7	PG-8	PG-9	PG-10	PG-11	PG-12	PG-13	PG-14	
Nb	106.2	149.3	78.8	88.7	490.3	128.4	147.7	180.3	173.6	159.5	119.5	79.0	35.2	20.4	44.9
Cs	1.0	1.0	1.0	1.3	0.8	3.9	1.0	1.0	0.9	1.1	0.9	0.7	0.9	0.9	0.9
Ba	6.5	5.5	1.5	6.7	60.5	206.8	6.5	3.4	1.3	0.8	1.4	675.6	1.5	1.7	226.2
Hf	102.1	67.0	73.2	150.2	18.9	9.8	69.3	47.3	57.1	171.9	49.7	9.8	331.7	541.2	294.3
Ta	1.8	7.1	1.9	2.0	12.2	4.0	6.6	2.7	2.6	6.6	2.0	2.9	2.0	0.5	1.8
Pb	24.2	31.1	24.6	28.8	4.3	10.1	22.6	20.7	15.4	39.3	41.4	2.7	18.7	11.7	11.0
Th	21.1	30.7	19.8	26.0	83.5	40.8	25.0	57.1	58.1	31.2	30.3	15.1	4.7	3.7	7.8
U	5.9	5.3	4.0	5.4	8.5	8.3	5.3	6.1	5.7	4.3	5.8	2.3	1.2	1.5	1.7

volcanic arc and oceanic-ridge granites mostly based on the content of high-field-strength elements (HFSE). The within-plate origin of the PG samples is substantiated by the Rb vs Y + Nb plot (Fig. 5f). the total-alkali silica (TAS) diagram (Le Maitre, 2002) of PG and enclaves shows that MMEs are alkaline occupying the basaltic field (Fig. 5g). The HMEs show mafic–felsic intermediate compositions occupying the trachyte–trachyandesite and phono-tephrite fields.

The Harker variation diagrams (Fig. 6) show the variation of major element oxides with silica as the magma differentiate in which Na_2O and K_2O increase, indicating a positive correlation during the evolution of PG pluton. The MgO, FeO, TiO_2 and CaO decrease with increasing silica. Al_2O_3 remains almost constant or slightly increases with differentiation. The K_2O content in FME ranges from 4.3 to 3.6 wt %, HME from 4.9 to 3.2 wt %, and MME from 2.2 to 1.4 wt %, indicating an overall decrease in K_2O content from FMEs to MMEs. The high Fe_2O_3 content in MME ranges from 10.95 to 11.48 wt %, which can be ascribed to the presence of mafic minerals. The Rb concentrations in the PG samples are generally high and vary from 136 to 278 ppm. This is concomitant with the high abundance of K_2O in the granite. Ba, which can also substitute to K, is less abundant, ranging from 32 to 132 ppm. The decrease in Ba content with increasing SiO_2 (Fig. 6) indicates the fractionation of K-feldspar during the crystallization of PG. The Rb contents are moderate, varying between 136 and 278 ppm. The Ca and Sr contents show decreasing trends with increasing SiO_2. The granite samples are also characterized by moderately high concentrations of U (4.2 to 20.5 ppm) and Th (35 to 55.5 ppm) along with HFSE such as Zr (85.5 to 356 ppm), Nb (99 to 216 ppm) and Y (79.6 to 201.8 ppm), and low concentrations of transition metal trace elements Ni (1.1 to 4 ppm), Cr (7.8 to 8.2 ppm) and Co (0.3 to 1.1 ppm). Trace element geochemistry indicates that the MME consist of relatively high N i (10.6 to 88 ppm), Cr (63 to 283 ppm) and Co (45 to 115 ppm). The HFSE contents of Zr (144 to 466 ppm) and Y (28 to 79 ppm) in MME show moderate abundances.

The PG samples are characterized by low to moderately fractionated REE patterns (Fig. 7a) with $(La/Yb)_N$ varying between 9.05 and 19.26. The PG samples are characterized by strong LREE fractionation $((La/Sm)_N = 3.91–5.0)$ with flat HREE $((Gd/Yb)_N = 0.7–3.3)$ patterns. The PG samples also exhibit negative Eu anomalies (Eu/Eu)*N ranging from 0.04 to 0.07. The chondrite-normalized (after Nakamura, 1974) REE patterns of xenolith, FME and HME are enriched in LREE and show prominent negative Eu anomalies (Fig. 7b, c and d), indicating a significant role of plagioclase fractionation from the parent magma. The chondrite-normalized REE patterns of the MME exhibit marginally enriched LREE and relatively depleted HREE (Fig. 7e). Low-amplitude negative to no Eu anomaly is observed in the MME, with the (Eu/Eu)*N ranging from 0.3 to 1.0. The primitive-mantle-normalized (after Sun & McDonough, 1989) multi-element diagram (Fig. 7f) of the PG samples shows prominent negative anomalies in Ba, Sr, P, Eu and Ti, while Th, U, Ce, Pr, Nb, Sm, Dy, Y and Nd show positive anomalies. The negative anomalies of Sr and Eu are related to the fractionation of plagioclase in the source region (Hanson, 1978). The negative anomalies of P and Ti reflect the fractionation of apatite and Fe–Ti oxides. The overall geochemical characteristics of the granites from PG pluton indicate its anorogenic, alkaline (A-type) nature (Whalen *et al.* 1987). The incompatible trace-element-normalized (after Sun & McDonough, 1989) multi-element diagrams (Fig. 7g, h and i) for the xenolith, FME and HME depict negative Ba, Sr and Ti anomalies and
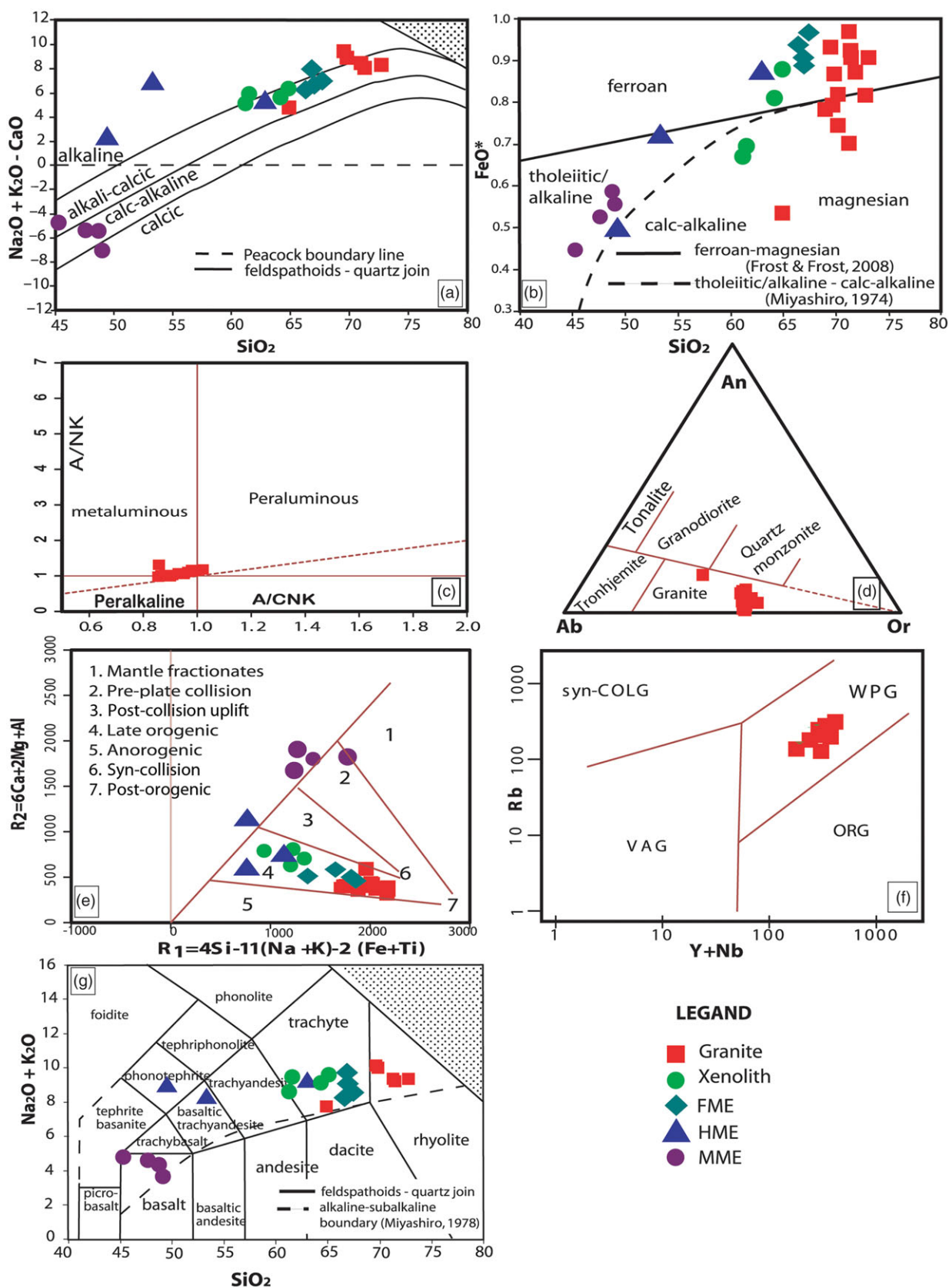
Fig. 5. (Colour online) (a) MALI vs silica diagram (Frost *et al.* 2001) showing alkali-calcic nature of Punugodu granite. (b) FeO* vs silica diagram (Frost & Frost, 2008) showing MME occupy the tholeiitic/alkaline field. (c) A/NK vs A/CNK diagram (Shand, 1943; Maniar & Piccoli, 1989) for granites and enclaves. (d) Normative anorthite (An)–albite (Ab)–orthoclase (Or) diagram (O'Connor, 1965). (e) R1–R2 tectonic classification diagram (after Batchelor & Bowden, 1985) showing the position of Punugodu granite in syn-collision to late orogenic tectonic setting, $R_1 = 4Si - 11(Na + K) - 2(Fe + Ti)$; $R_2 = 6Ca + 2Mg + Al$. (f) Rb vs (Y + Nb) diagram (after Pearce *et al.* 1984, 1996) showing the position of Punugodu granite in WPG. (g) Total-alkali silica (TAS) diagram (Le Maitre, 2002) of Punugodu samples. Note: The symbols denoting granite, xenoliths, FME. HME and FME are applicable for all geochemical plots.
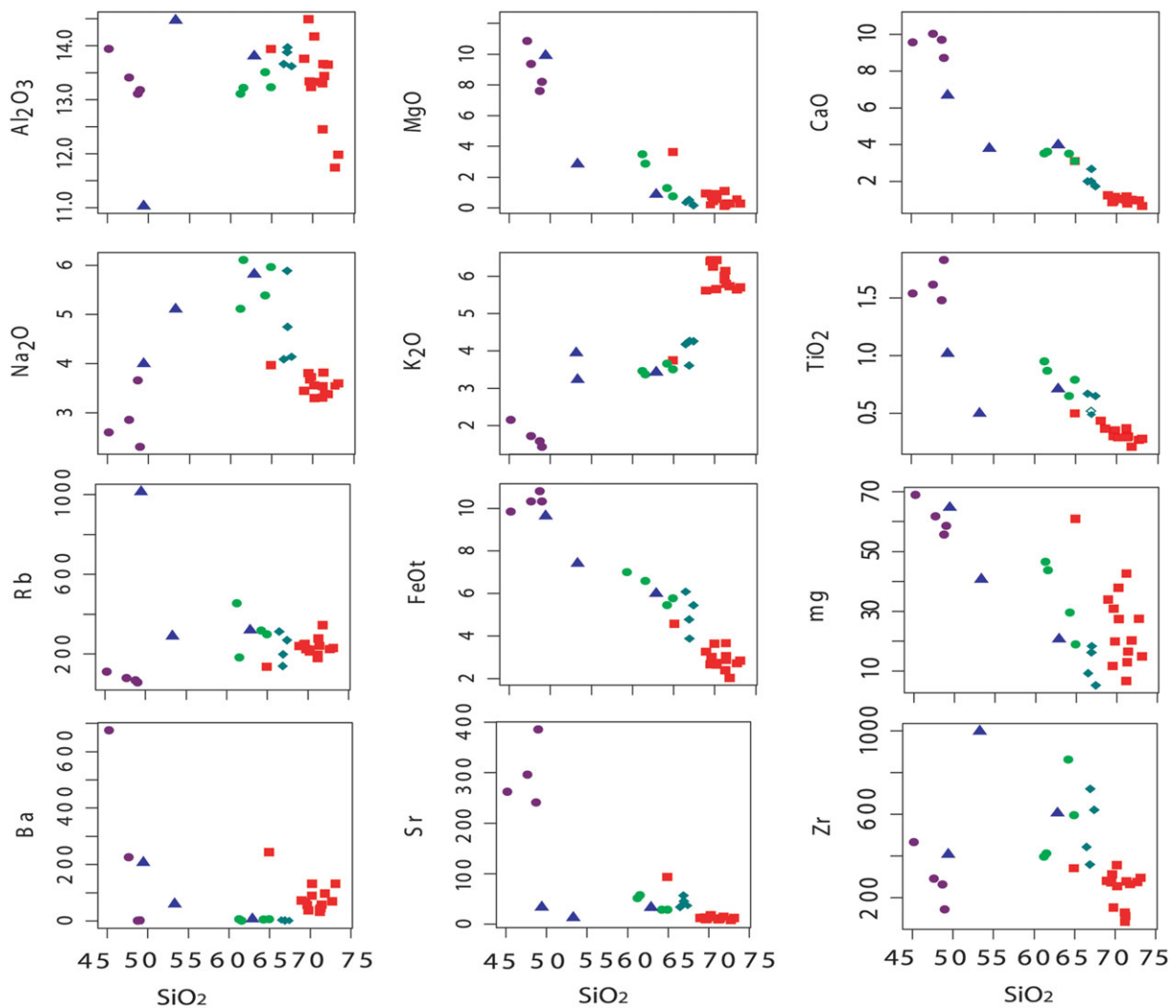
Fig. 6. (Colour online) Harker's variation diagram showing the variation of major oxides and trace elements with SiO_2.

positive Rb anomalies, wheareas the MMEs show negative Ba with constant Sr and Ti and positive Rb anomaly (Fig. 7j).

5.b. Zircon U–Pb geochronology

The PG-8 granite sample with abundant zircons is chosen for U–Pb geochronology. Zircon grains extracted from this sample are well-developed euhedral grains, typically 80–200 µm long with aspect ratios of 2:1 to 3:1. They show concentric growth zoning typical of magmatic zircons (Corfu *et al.* 2003), and, in a few cases, convolute zoning suggests crystallization from melts. The CL images of representative zircon grains are given in Figure 8. The zircon grains show well-preserved prismatic terminations suggesting limited magmatic resorption. Most of the zircons have systematic growth zoning from core to rim. Luminescent outer rims are rare, suggesting a general lack of metamorphic over-growth. Rarely, an effect of alteration is evident in the development of bright luminescent patches across growth zoning.

In general, the laser spots were placed in homogeneous interiors of zircons, avoiding older (inherited) domains and visibly altered segments. *In situ* laser-ablation ICP-MS U–Th–Pb isotopic data for individual laser spots in zircons from the sample are given in Table 2. Age calculations are discussed based on a $^{207}Pb/^{235}U$ vs $^{206}Pb/^{238}U$ concordia diagram (Fig. 9). The concordant zircon grains have U content between 7.6 and 384 ppm with an average of 95.4 ppm, Th ranging from 5.6 ppm to 427.7 ppm with an average 75.6 ppm, and Th/U = 0.43 to 1.49, attesting to their typical magmatic character (Rubatto, 2002). The zircons yield a concordia upper intercept U–Pb age of 1257 ± 6 Ma (2σ errors), MSWD = 7.5. We interpret 1257 ± 6 Ma concordia upper intercept age as the time of emplacement and magmatic crystallization of the Punugodu granite pluton.

6. Discussion

6.a. Genetic type and tectonic setting

The Punugodu granite is mineralogically an alkali feldspar granite and is characterized by high SiO_2 and $Na_2O + K_2O$. The average Fe number for PG is 0.83, indicating its ferron nature. In the A/NK vs A/CNK diagram (Fig. 5c), the sample of PG granite falls at the juncture of metaluminous and peralkaline fields. Based on the major oxide geochemistry, alkali feldspar granites of ferroan affinity, metaluminous and peralkaline by virtue of their alumina saturation, have been recognized as alkaline (A-type) granites (e.g. Frost & Frost, 2011). Whalen *et al.* (1987) proposed several
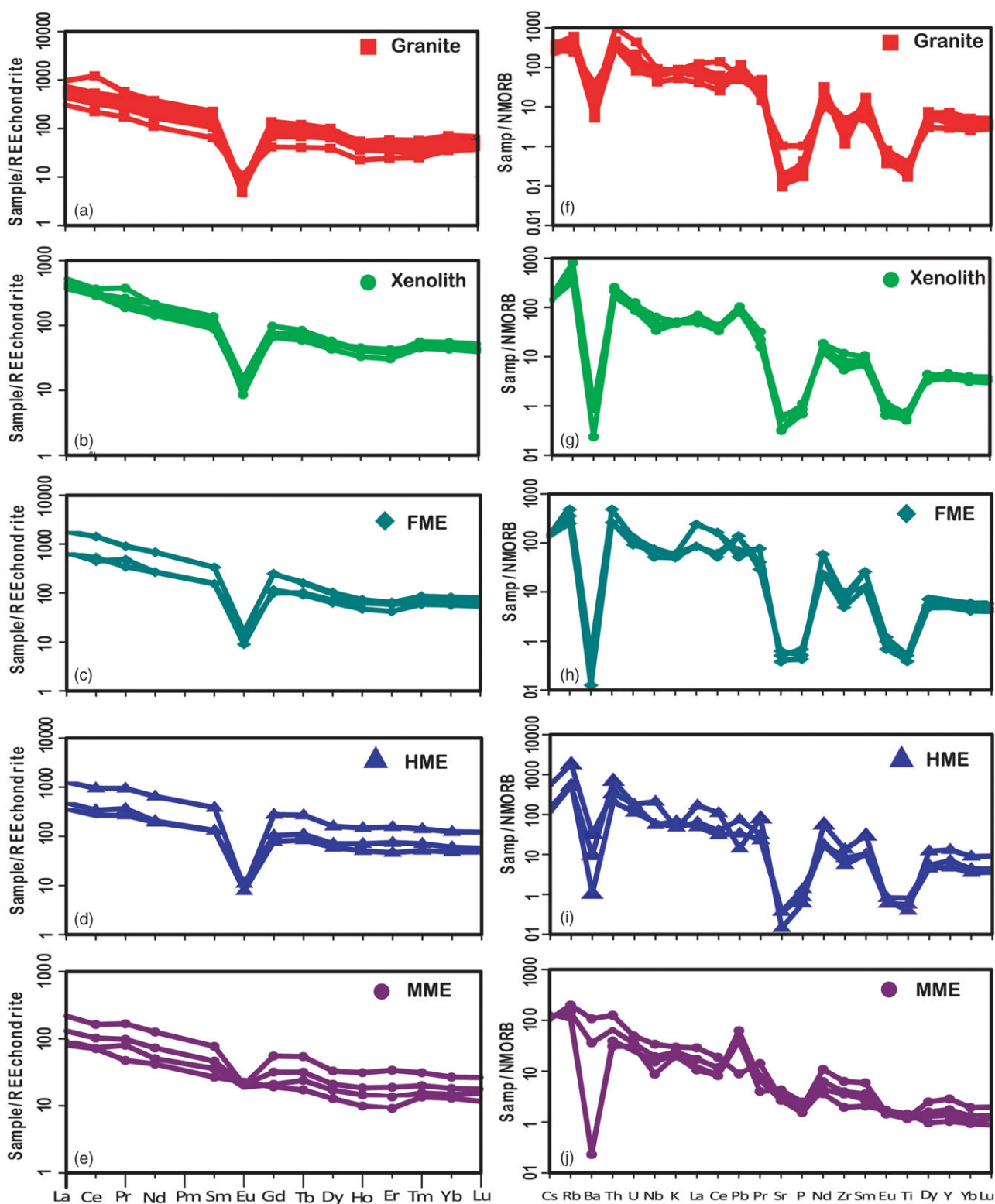
Fig. 7. (Colour online) Chondrite-normalized (normalized values after Nakamura, 1974) REE and primitive-mantle-normalized (values after Sun & McDonough, 1989) multi-element diagrams of granite and enclaves.

discrimination diagrams to distinguish the A-type granite from other granite types such as I-, S- and M-types. The 10 000 * Ga/Al values vary with Zr, Nb and FeO/MgO content, and $Na_2O + K_2O$ can discriminate A-type granites. The separating line

in the discrimination diagram is at Ga/Al > 2.6. All the samples of the PG are positioned exclusively in the field of A-type granite in the Zr and Nb vs Ga/Al diagrams (Fig. 10a and b). The high concentration of $Na_2O + K_2O$, high Fe number and enriched
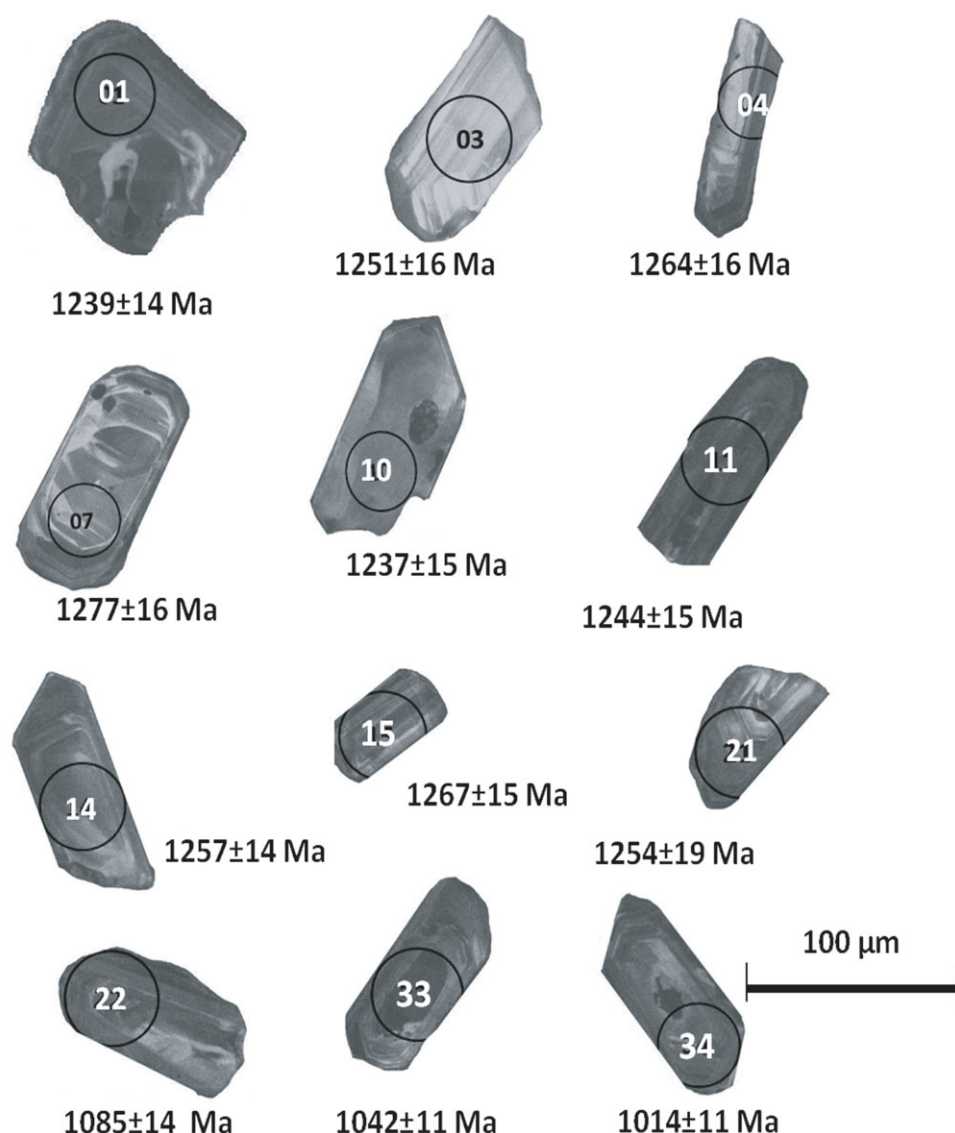
Fig. 8. (Colour online) Cathodoluminescence images of zircon grains, Punugodu granite.

HFSE (Zr, Nb and Y) contents along with enriched LREE in the PG correspond with A-type granites (Whalen *et al.* 1987; Eby, 1992).

Eby (1992) classified the A-type granites into subtypes A1 and A2, based on the Y/Nb ratio. The A1 group (Y/Nb < 1.2) was interpreted as alkaline magma derived from an oceanic island basalt (OIB)-like source in a proper anorogenic within-plate setting. The PG shows Y/Nb ratios of <1.2, ranging from 0.6 to 0.91, indicating its A1-type granite, commonly emplaced in an extensional regime in an anorogenic within-plate setting. This is further corroborated by ternary Y–Nb–3Ga and Y–Nb–Zr/4 plots (Fig. 10c and d) for the PG samples (Eby, 1992).

Pearce *et al.* (1984), based on the compilation of >600 analyses of felsic rocks, divided the granites into four major tectonic groups: ocean ridge granite (ORG), volcanic arc granite (VAG), within-plate granite (WPG) and collisional granite (COLG). In the Rb vs Y + Nb graph, the PG clearly plots within the WPG field (Fig. 5f). This setting for some A-type granites has also been described from occurrences elsewhere in the world (e.g. Eby, 1992). The prominent positive anomalies in granite and enclave samples observed for Rb, Th, U, Ce, Pr, Nb, Sm, Dy, Y and Nd are typical of anorogenic-related granite magmatism.

6.b. Magma mingling and mixing

The presence of oval-, sub-oval- and elliptical-shaped ME hosted in the PG indicates the hybridizing magma system (Kumar *et al.* 2004). The host PG and the enclaves such as xenoliths and FME show a continuous variation in SiO_2 concentrations, producing tightly linear to slightly curved trends on Harker variation diagrams (Fig. 6), strong evidence for a genetic link between them. However, the observed wide composition of HME may be due to the chemical mixing between two contrasting magma end-members in varying proportions (Kumar & Rino, 2006). The fine-grained, igneous-textured mafic to hybrid ME from I- and A-type granites has been considered to represent mafic and/or hybrid magma components added to intermediate or felsic magma chambers (e.g. Holden *et al.* 1987; Vernon *et al.* 1988; Bedard, 1990; Didier & Barbarin, 1991; Bonin, 2004; Yang *et al.* 2004;

Table 2. LA-ICP-MS U–Th–Pb isotopic data and calculated ages for zircons from the Punugodu granite pluton

Analysis_#	Th ppm	U ppm	Th/U	Isotopic ratios					Age (Ma)				% Conc
				$^{207}Pb/^{235}U$	2σ	$^{206}Pb/^{238}U$	2σ	rho	$^{207}Pb/^{206}Pb$	1σ	$^{206}Pb/^{238}U$	1σ	
PG zircons													
UVB-01	2.97	5.39	0.55	2.48712	0.0896	0.2119	0.0027	0.355	1333.8	47.94	1239	14.43	93
UVB-02	3.73	3.67	1.02	2.54174	0.1523	0.2009	0.0031	0.259	1464.2	69.77	1180.1	16.74	81
UVB-03	1.57	1.68	0.94	2.51184	0.1322	0.2141	0.0031	0.278	1421.3	63.37	1250.7	16.63	88
UVB-04	2.16	3.13	0.69	2.506	0.1319	0.2167	0.0032	0.277	1342	64.23	1264.3	16.74	94
UVB-06	4.63	7.04	0.66	2.53878	0.1149	0.2118	0.0029	0.307	1403.5	57.29	1238.4	15.62	88
UVB-07	1.41	2.29	0.62	2.53138	0.1291	0.2192	0.0032	0.284	1329.9	63.92	1277.4	16.76	96
UVB-08	4.44	9.36	0.47	2.2479	0.1333	0.1769	0.0028	0.267	1495.7	72.54	1050.1	15.35	70
UVB-10	3.11	5.23	0.59	2.61489	0.1054	0.2115	0.0029	0.335	1378.4	55.2	1236.6	15.15	90
UVB-11	6.07	7.16	0.85	2.51741	0.1131	0.2129	0.0030	0.312	1373.5	60.15	1244.4	15.82	91
UVB-12	11.33	7.41	1.53	2.46729	0.1101	0.2073	0.0029	0.314	1379.7	60.65	1214.2	15.49	88
UVB-13	2.19	3.17	0.69	2.59442	0.1152	0.2126	0.0029	0.304	1410.7	54.4	1242.8	15.28	88
UVB-14	2.70	4.38	0.62	2.58689	0.0982	0.2152	0.0028	0.339	1373.3	48.91	1256.6	14.69	92
UVB-15	5.93	7.03	0.84	2.55049	0.1226	0.2172	0.0030	0.289	1381	58.59	1267.3	15.99	92
UVB-17	7.41	10.41	0.71	2.38887	0.0926	0.1798	0.0024	0.337	1593.1	49.83	1066	12.86	67
UVB-18	13.44	14.91	0.90	2.20437	0.0684	0.1791	0.0022	0.396	1402.4	44.6	1062.3	12.05	76
UVB-19	10.41	12.40	0.84	2.58039	0.0986	0.2011	0.0026	0.338	1465.7	50.67	1181.4	13.96	81
UVB-20	4.98	7.23	0.69	2.41636	0.0966	0.1829	0.0024	0.330	1571.2	52.33	1082.9	13.15	69
UVB-21	3.42	2.35	1.45	2.51246	0.1883	0.2147	0.0038	0.233	1441.6	86.77	1253.8	19.9	87
UVB-22	4.25	4.43	0.96	2.29574	0.1139	0.1833	0.0026	0.286	1395.7	63.96	1084.9	14.17	78
UVB-24	3.42	5.62	0.61	2.51595	0.2065	0.2091	0.0038	0.223	1371.2	95.6	1223.9	20.4	89
UVB-26	5.74	14.00	0.41	2.15522	0.0801	0.1794	0.0022	0.336	1380.2	49.75	1063.4	12.25	77
UVB-27	20.21	11.32	1.79	2.04652	0.0650	0.1590	0.0019	0.378	1386.4	44.92	951.4	10.61	69
UVB-28	16.71	23.89	0.70	2.17854	0.0907	0.1822	0.0024	0.311	1346.1	54.6	1078.7	12.86	80
UVB-29	34.48	33.68	1.02	2.10274	0.0678	0.1721	0.0021	0.375	1400.8	45.66	1023.7	11.41	73
UVB-30	10.94	11.12	0.98	2.25221	0.1142	0.1828	0.0026	0.275	1370.5	63.43	1082	13.92	79
UVB-31	29.98	40.14	0.75	2.1384	0.0708	0.1712	0.0021	0.367	1444	47.03	1018.9	11.46	71
UVB-32	11.17	16.27	0.69	2.06116	0.0838	0.1744	0.0023	0.317	1356.2	55.08	1036.4	12.37	76
UVB-33	16.56	21.94	0.75	2.13549	0.0722	0.1755	0.0022	0.362	1410.4	48.57	1042.5	11.78	74
UVB-34	6.19	9.48	0.65	2.14217	0.0831	0.1703	0.0022	0.329	1436.4	53.56	1013.5	11.96	71
UVB-35	3.15	4.86	0.65	2.26149	0.0889	0.1889	0.0024	0.326	1401.9	54.33	1115.5	13.1	80
UVB-36	149.88	55.01	2.72	1.61357	0.0579	0.1109	0.0014	0.349	1545.2	51.84	678.2	8.09	44

Kumar, 2020). Silica contents in the MEs indicate a broad bimodal distribution. The SiO_2 contents in MME and in some HME range from 45 to 53 %, while the SiO_2 contents in FME and granite samples show a relatively wide variation from 61 to 73 %, separated by a silica gap of *c.* 8 wt %. The relative enrichment of Ni and Cr in the MME and HME samples suggests that they might have formed from mantle-derived mafic and mafic–felsic (hybrid) magmas respectively, injected into the crystallizing host magma chamber as described elsewhere (Kumar *et al.* 2017). Notable variation in the Ba content in some of the MME samples is perhaps due to

geochemical heterogeneities in the feldspars during magma mixing (e.g. Bonin, 2004; Słaby *et al.* 2011).

6.c. Temperature and pressure

Zirconium saturation level (ppm) as a function of cationic ratio M = (Na + K + 2Ca)/(Al. Si) (Watson & Harrison 1983) shows two different ranges of crystallization temperatures for granite, 750–800° C and 850–900° C (Fig. 10e). This may be because of crystallization of zircon right from liquidus to solidus. Based on
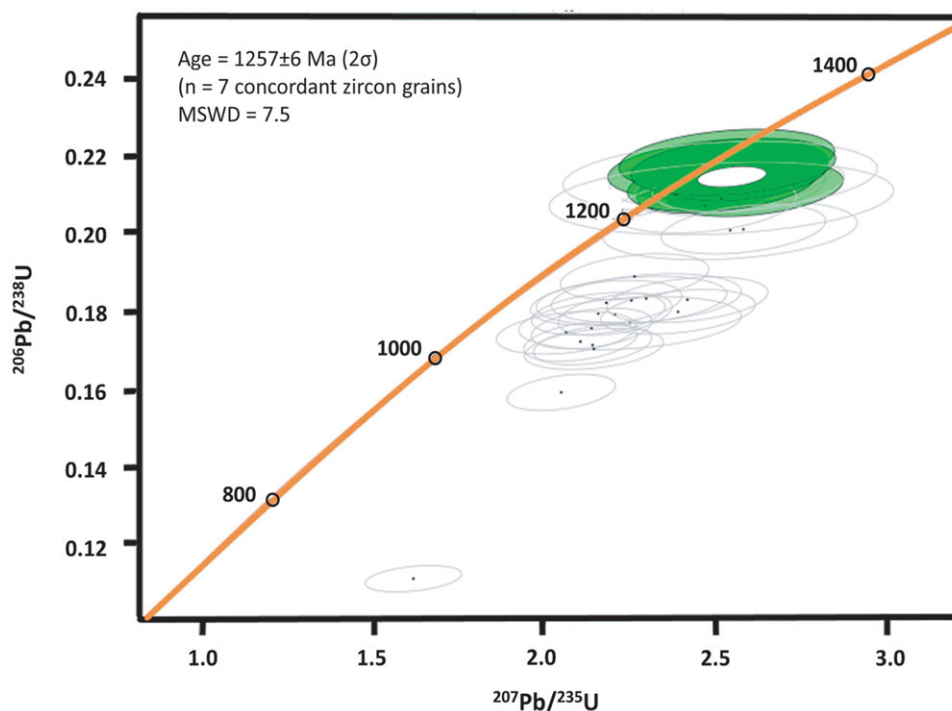
Fig. 9. (Colour online) Concordia age diagram of zircon using LA-ICP-MS U–Th–Pb isotopic data on the Punugodu granite.

the Cross, Iddings, Pirsson and Washington norm, the normative Qz–Ab–Or ternary diagram (Johannes & Holtz 1996), the granite's crystallization pressure varies from 1 to 2 GPa (Fig. 10f).

6.d. Age constraints

The southeastern margin of India has witnessed several extensional as well as subduction events. The first extension- and rift-related Palaeoproterozoic anorogenic magmatism occurred at 1.9 Ga due to mantle diapir or plume. This rifting would have allowed an open ocean to form on the eastern margin of the EDC. The occurrence of 1.85 Ga Kandra and 1.33 Ga Kanigiri ophiolite affinity rocks in the NSB indicates the repeated subduction-related tectonic convergence. The Mesoproterozoic rift-related magmatism occurred in PAkP, resulting in the emplacement of 1321 Ma Elchuru nepheline syenite, 1334 Ma Purimetla gabbro, 1352 Ma Errakonda ferrosyenite and 1356 Ma Uppalapadu nepheline syenite. We find that the plutons emplaced around the Kanigiri area, such as 1284 Ma Kanigiri granite, 1256 ± 6 Ma Punugodu granite (present study) and 1251 Ma Peddacharlopalle gabbro, are relatively younger (~ 80 Ma) than the PAkP alkaline rocks. There is a sort of trend of emplacement age of plutons ending towards the south. Sain & Saha (2018) have opined that the 1284 Ma Kanigiri granite intruded the 1334 Ma Kanigiri Ophiolite and thus affirmed their post-tectonic emplacement. In line with the above argument, the studied PG with age 1257 ± 6 Ma is so far the youngest member of felsic plutons in NSB, formed and emplaced in an extensional environment. The nearly 30 Ma gap between Kanigiri and Punugodu granites has further refined the age of felsic magmatism, thus indicating the existence of a plutonic trinity (alkaline/felsic/mafic) in this belt and implications on the crustal growth during the waning stage of Columbia supercontinent fragmentation in the NSB of the EDC.

7. Conclusions

A new age of 1257 ± 6 Ma for the Punugodu granite located in the NSB of Southern India is reported. The geochemical characters of the PG broadly align its nature with the metaluminous, alkali-calcic, within-plate A-type granite. Xenoliths hosted in PG are pre-existing felsic metavolcanic rock fragments. The MME and HME represent distinct batches of mantle-derived mafic and mafic–felsic (hybrid) magmas respectively that injected, mingled and undercooled within the felsic host PG magma. The FME appears to be early crystallized cogenetic facies of the PG pluton. Y/Nb ratios (Y/Nb < 1.2) indicate an oceanic island basalt (OIB)-like source for the PG melts formed in an anorogenic within-plate setting. Field observations suggests that PG (*c.* 1257 Ma) has intrusive relationships with the Mesoproterozoic (*c.* 1334 Ma) KO of oceanic arc supra-subduction affinity. The PG probably emplaced during an extensional tectonic environment along the western margin of the Neoarchaean NSB in the eastern Dharwar Craton.

Conflict of interest. None.

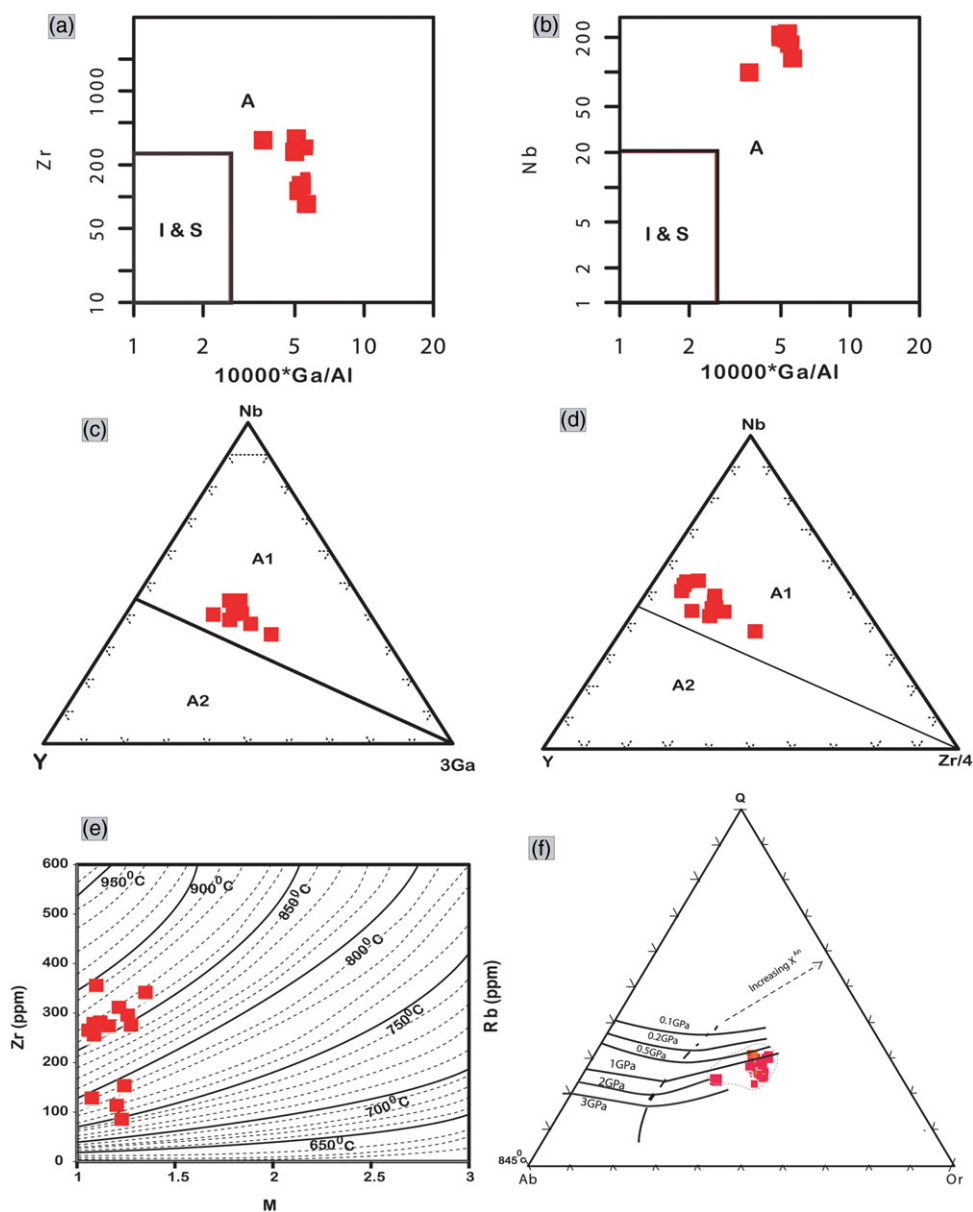**Fig. 10.** (Colour online) **(a)** Zr and **(b)** Nb vs 10 000 * Ga/Al discrimination diagrams of Whalen *et al*. (1987) showing the A-type nature of the Punugodu granite. (c, d) Chemical classification diagrams of A-type granite (after Eby, 1992): (c) Nb–Y–3Ga ternary diagram and (d) Nb–Y–Zr/4 ternary diagram. (e) Zirconium saturation level (ppm) as a function of cationic ratio M = (Na + K + 2Ca)/(Al. Si) (Watson & Harrison 1983) showing crystallization temperature of granite. (f) The normative Qz–Ab–Or ternary diagram shows the pressure of crystallization of PG (Johannes & Holtz 1996).

References

Alling HL (1938) Plutonic perthites. *Journal of Geology* **46**, 142–65.

Andersen T (2002) Correction of common lead in U–Pb analyses that do not report [204]Pb. *Chemical Geology* **192**, 59–79.

Anderson O (1928) The genesis of some type of feldspar from granite pegmatites. *Norsk Geologisk Tidsskrift* **10**, 116–207.

Babu EVSSK, Bhaskar Rao YJ and Vijaya Kumar T (2009) In-situ U-Pb and Hf-isotopic characterization of GJ-1 zircon by laser ablation ICP-MS and MC-ICP-MS. In *Eleventh ISMAS Triennial International Conference on Mass Spectrometry* (eds SK Aggarwal *et al.*), 511–14. Mumbai: Indian Society for Mass Spectrometry.

Barbarin B and Didier J (1991) Conclusions: enclaves and granite petrology. In *Enclaves and Granite Petrology* (eds J Didier and B Barbarin), pp. 545–49. Amsterdam: Elsevier.

Batchelor RA and Bowden P (1985) Petrogenetic interpretation of granitoid rock series using multicationic parameters. *Chemical Geology* **48**, 43–55.

Bedard J (1990) Enclaves from the A-type granite of the mégantic complex, White Mountain magma series: clues to granite magma genesis. *Journal of Geophysical Research* **95**, 17797–819.

Black R and Liégeois JP (1993) Cratons, mobile belts, alkaline rocks and continental lithospheric mantle: the Pan-African testimony. *Journal of the Geological Society, London* **150**, 89–98.

Bonin B (1991) The enclaves of alkaline anorogenic granites: an overview. In *Enclaves and Granite Petrology* (eds J Didier and B Barbarin), pp. 179–89. Amsterdam: Elsevier.

Bonin B (1998) Alkaline rocks and geodynamics. *Turkish Journal of Earth Sciences* **7**, 105–18.

Bonin B (2004) Do coeval mafic and felsic magmas in post-collisional to within-plate regimes necessarily imply two contrasting, mantle and crust, sources? A review. *Lithos* **78**, 1–24.

Bonin B (2007) A-type granites and related rocks: evolution of a concept, problems and prospects. *Lithos* **97**, 1–29.

Chaudhuri AK, Saha D, Deb GK, Deb SP, Mukherjee MK and Ghosh G (2002) The Purana basins of southern cratonic province of India: a case for Mesoproterozoic fossil rifts. *Gondwana Research* **5**, 23–33.

Clemens JD, Holloway JR and White AJR (1986) Origin of A-type granites: experimental constraints. *American Mineralogist* **71**, 317–24.

Collins WJ, Beams SD, White AJR and Chappell BW (1982) Nature and origin of A-type granites with particular reference to Southeastern Australia. *Contributions to Mineralogy and Petrology* **80**, 189–200.

Corfu F, Hanchar JM, Hoskin PWO and Kinny P (2003) Atlas of zircon textures. *Reviews in Mineralogy & Geochemistry* **53**, 469–95.

Dall'Agnol R, Frost CD and Rämö OT (2012) IGCP Project 510 "A-type Granites and Related Rocks through Time": project vita, results, and contribution to granite research. *Lithos* **151**, 1–16. doi:10.1016/j.lithos.2012.08.003.

De la Roche, H, Leterrier, P, Grandclaude, P and Marshall, M (1980) A classification of volcanic and plutonic rocks using R1-R2 diagrams and major element analysis: its relationship with current nomenclature. *Chemical Geology* **29**, 183–210.

Dharma Rao CV and Reddy UVB (2007) Petrology and geochemistry of Paleoproterozoic A-type granite at Kanigiri in the Nellore-Khammam Schist Belt, Andhra Pradesh, India. *Journal of Asian Earth Sciences* **30**, 1–19.

Dharma Rao CV, Santosh M and Dong Y (2012) U-Pb zircon chronology of the Pangidi-Kondapalle layered intrusion, Eastern Ghat Belt, India: constraints on Mesoproterozoic arc magmatism in a convergent margin setting. *Journal of Asian Earth Sciences* **49**, 362–75. doi: 10.1016/j.jseaes.2011.07.005.

Dharma Rao CV, Santosh M and Yuan-Bao W (2011) Mesoproterozoic ophiolitic mélange from the SE periphery of the Indian plate: U-Pb zircon ages and tectonic implications. *Gondwana Research* **19**, 384–401.

Didier J and Barbarin B (eds) (1991) *Enclaves and Granite Petrology Developments in Petrology*. Amsterdam: Elsevier, 625 pp.

Divakara Rao V, Rama Rao P and Subba Rao MV (1999) The Ghingee grannite,Tamilnadu, South India: geochemistry and petrogenesis. *Gondwana Research* **2**, 117–26.

Dobmeier C, Lutke S, Hammerschmidt K and Mezger K (2006) Emplacement and deformation of the Vinukonda meta-granite (Eastern Ghats, India): implications for the geological evolution of peninsular India and for Rodinia reconstructions. *Precambrian Research* **146**, 165–78.

Dobmeier C and Raith MM (2003) Crustal architecture and evolution of the Eastern Ghats belt and adjacent regions of India. In *Proterozoic East Gondwana: Supercontinent Assembly and Breakup* (eds Yoshida M, Windley BF and Dasgupta S), pp. 145–68. Geological Society of London, Special Publication no. 206..

Eby GN (1990) The A-type granitoids: a review of their occurrence and chemical characteristics and speculations on their petrogenesis. *Lithos* **26**, 115–34.

Eby GN (1992) Chemical subdivision of the A-type granitoids: petrogenetic and tectonic implications. *Geology* **20**, 641–4.

Eby GN and Kochhar N (1990) Geochemistry and petrogenesis of the Malani Igneous Suite, Northern India. *Journal of the Geological Society of India* **36**, 109–30.

French JE, Heaman LM, Chacko T and Srivastava RK (2008) 1891–1883 Ma Southern Bastar–Cuddapah mafic igneous events, India: a newly recognized large igneous province. *Precambrian Research* **160**, 308–22.

Frost BR, Barnes CG, Collins WJ, Arculus RJ, Ellis DJ and Frost CD (2001) A geochemical classification for granitic rocks. *Journal of Petrology* **42**, 2033–48.

Frost BR and Frost CD (2008) A geochemical classification for feldspathic igneous rocks. *Journal of Petrology* **49**, 1955–69.

Frost CD and Frost BR (2011) On ferroan (A-type) granitoids: their compositional variability and modes of origin. *Journal of Petrology* **52**, 39–53.

Frost CD, Frost BR, Chamberlain KR and Edwards BR (1999) Petrogenesis of the 1.43 Ga Sherman batholith, SE Wyoming, USA: a reduced, rapakivi-type anorogenic granite. *Journal of Petrology* **40**, 1771–802.

Gupta JN, Pandey BK, Chabria T, Banerjee DC and Jayaram KMV (1984) Rb-Sr geochronological studies on the granites of Vinukonda and Kanigiri, Prakasam District, Andhra Pradesh, India. *Precambrian Research* **26**, 105–9.

Hanson GN (1978) The application of trace elements to the petrogenesis of igneous rocks of granitic composition. *Earth and Planetary Science Letters* **38**, 26–43.

Henderson B, Collins AS, Payne J, Forbes C and Saha, D (2014) Geologically constraining India in Columbia: the age, isotopic provenance and geochemistry of the protoliths of the Ongole Domain, Southern Eastern Ghats, India. *Gondwana Research* **26**, 888–906.

Holden P, Halliday AN and Stephens WE (1987) Neodymium and strontium isotope content of microdiorite enclaves points to mantle input to granitoid production. *Nature* **330**, 53–6.

Johannes W and Holtz F (1996) *Petrogenesis and Experimental Petrology of Granitic Rocks.* Berlin: Springer.

Kerr A and Fryer BJ (1993) Nd isotopic evidence for crust–mantle interaction in the generation of A-type granitoid suites in Labrador, Canada. *Chemical Geology* **104**, 39–60.

King PL, White AJR, Chappell BW and Allen CM (1997) Characterization and origin of aluminous A-type granites from the Lachlan fold belt, southeastern Australia. *Journal of Petrology* **38**, 371–91.

Kovach VP, Simmat R, Rickers K, Berezhnaya NG, Salnikova EB, Dobmeier C, Raith MM, Yakovleva SZ and Kotov AB (2001) The Western Charnockite Zone of the Eastern Ghats Belt, India: an independent crustal province of late Archaean (2.8 Ga) and Paleoproterozoic (1.7–1.6 Ga) terrains. *Gondwana Research* **4**, 666–7.

Krishna AK, Murthy NN and Govil PK (2007) Multielement analysis of soils by wavelength-dispersive X-ray fluorescence spectrometry. *Atomic Spectroscopy* **28**, 202–14.

Kumar S (1995) Microstructural evidence of magma quenching inferred from microgranular enclave hosted in Hodruša granodiorite, western Carpathians. *Geologica Carpathica* **46**, 379–82.

Kumar S (2010) Mafic to hybrid microgranular enclaves in the granitoids of Ladakh batholith, Northwest Higher Himalaya: implications on calc-alkaline magma chamber processes. *Journal of the Geological Society of India* **76**, 5–25.

Kumar S (2020) Schedule of mafic to hybrid magma injections into crystallizing felsic magma chambers and resultant geometry of enclaves in granites: new field and petrographic observations from Ladakh Batholith, Trans-Himalaya, India. *Frontiers in Earth Science* **8**, 551097.

Kumar S, Gupta S, Sensarma S and Bhutani R (2020) Proterozoic felsic and mafic magmatism in India: implications to crustal evolution through crust-mantle interactions. *Episodes* **43**, 203–30.

Kumar S, Pieru T, Rino V and Hayasaka Y (2017). Geochemistry and U–Pb SHRIMP zircon geochronology of microgranular enclaves and host granitoids from South Khasi Hills of the Meghalaya Plateau, NE India: evidence of synchronous mafic–felsic magma mixing–fractionation and diffusion in a post-collision tectonic environment during the Pan-African orogenic cycle. In *Crustal Evolution of India and Antarctica: The Supercontinent Connection* (eds S Bose, P Seth and N Dasgupta), pp. 253–89. *Geological Society of London, Special Publication* no. **457**. doi:10.1144/SP457.10.

Kumar S and Rino V (2006) Mineralogy and geochemistry of microgranular enclaves in Palaeoproterozoic Malanjkhand Granitoids, central India: evidence of magma mixing, mingling, and chemical equilibration. *Contributions to Mineralogy and Petrology* **152**, 591–609.

Kumar S, Rino V and Paul AB (2004) Field evidence of magma mixing from microgranular enclaves hosted in palaeoproterozoic Malanjkhand Granitoids, Central India. *Gondwana Research* **7**, 539–48.

Le Maitre, RW (2002) *Igneous Rocks: A Classification and Glossary of Terms*, second edition. Cambridge: Cambridge University Press, 236 pp.

Leelanandam C, Burke K, Ashwal LD and Webb SJ (2006) Proterozoic mountain building in Peninsular India: an analysis based primary on alkaline rock distribution. *Geological Magazine* **143**, 195–212.

Li H, Watanabe K and Yonezu K (2014) Geochemistry of A-type granites in the Huangshaping polymetallic deposit (South Hunan, China): implications for granite evolution and associated mineralization. *Journal of Asian Earth Sciences* **88**, 149–67.

Litvinovsky BA, Jahn BM, Zanvilevich AN, Saunders A, Poulain S, Kuzmin DV, Reichow MK and Titov AV (2002) Petrogenesis of syenite-granite

suites from the Bryansky complex (Transbaikalia, Russia): implications for the origin of A-type granitoid magmas. *Chemical Geology* **189**, 105–33.

Loiselle MC and Wones DR (1979) Characteristics and origin of anorogenic granites. *Geological Society of America Abstracts with Programs* **11**, 468.

Maniar PD and Piccoli DR (1989) Tectonic discrimination of granitoids. *Geological Society of America Bulletin* **101**, 635–43.

Manikyamba C, Santosh M, Chandan Kumar B, Rambabu S, Tang L, Saha A, Khelen AC, Ganguly S, Dhanakumar Singh Th and Subba Rao DV (2016) Zircon U-Pb geochronology, Lu-Hf isotope systematics, and geochemistry of bimodal volcanic rocks and associated granitoids from Kotri Belt, Central India: implications for Neoarchean–Paleoproterozoic crustal growth. *Gondwana Research* **38**, 318–33.

Meert JG, Pandit MK, Pradhan VR, Banks J, Sirianni R, Stroud M, Newstead B and Gifford J (2010) Precambrian crustal evolution of Peninsular India: a 3.0 billion year odyssey. *Journal of Asian Earth Sciences* **39**, 483–515.

Mingram B, Trumbull RB, Littman S and Gerstenberger H (2000) A petrogenetic study of anorogenic felsic magmatism in the Cretaceous Paresis ring complex, Namibia: evidence for mixing of crust and mantle-derived components. *Lithos* **54**, 1–22.

Miyashiro A (1974) Volcanic rock series in Island arcs and active continental margins. *American Journal of Science* **274**, 321–355.

Miyashiro A (1978) Nature of alkalic volcanic rock series. *Contributions to Mineralogy and Petrology* **66**, 91–104.

Mushkin A, Navon O, Halicz L, Hartmann G and Stein M (2003) The petrogenesis of A-type magmas from the Amram Massif, southern Israel. *Journal of Petrology* **44**, 815–32.

Nakamura N (1974) Determination of REE, Ba, Mg, Na and K in carbonaceous and ordinary chondrites. *Geochimica et Cosmochimica Acta* **38**, 757–75.

Narshimha Ch, Reddy UVB, Sesha Sai VV and Subramanyam KSV (2018) Petrological and geochemical characterisation of the Punugodu Granite Pluton Nellore Schist Belt; implications for Proterozoic anorogenic granite magmatism in the Eastern Dharwar Craton, Southern India. *Journal of the Indian Geophysical Union* **22**, 187–97.

O'Connor JT (1965) A classification for quartz-rich igneous rocks based on feldspar ratios. *US Geological Survey Professional Paper* 525-B, 79 pp.

Patiño Douce AE (1997) Generation of metaluminous A-type granites by low-pressure melting of calc-alkaline granitoids. *Geology* **25**, 743–6.

Pearce JA, Harris NBW and Tindle AG (1984) Trace element discrimination diagrams for the tectonic interpretation of granitic rocks. *Journal of Petrology* **25**, 956–83.

Pearce NJG, Westgate JA and Perkins WT (1996) Developments in the analysis of volcanic glass shards by laser ablation ICP-MS: quantitative and single internal standard-multielement methods. *Quaternary International* **36**, 213–27.

Perugini D, Valentini L and Poli G (2007) Insights into magma chamber processes from the analysis of size distribution of enclaves in lava flows: a case study from Volcano Island (Southern Italy). *Journal of Volcanology and Geothermal Research* **166**, 193–203.

Raman PK and Murthy VN (1997) *Geology of Andhra Pradesh*. Bangalore: Geological Society of India.

Rao ADP, Rao KN and Murthy YGK (1988) Gabbro-Anorthosite-Pyroxinite complexes and alkaline rocks of Chimakurti-Elchuru area, Prakasam District, Andhra Pradesh. *Records of the Geological Survey of India* **116**, 1–20.

Ratnakar J and Leelanandam C (1985) The Purimetla gabbros, Prakasam District, Andhra Pradesh, India. *Journal of Earth System Science* **94**, 305–13.

Ratnakar J and Vijaya Kumar K (1995) Petrogenesis of quartz-bearing syenite occurring within nepheline syenite of the Elchuru Alkaline Complex, Prakasam Province, Andhra Pradesh. *Journal of the Geological Society of India* **46**, 611–8.

Ravikant V (2010) Palaeoproterozoic (~1.9 Ga) extension and breakup along the eastern margin of the Eastern Dharwar Craton, SE India: new Sm–Nd isochron age constraints from anorogenic mafic magmatism in the Neoarchean Nellore greenstone belt. *Journal of Asian Earth Sciences* **37**, 67–81.

Reddy UVB and Sesha Sai VV (2003) Occurrence of a rare rhyodacite from the Kanigiri area, Prakasam district, Andhra Pradesh. *Journal of the Indian Academy of Sciences* **46**, 25–7.

Rubatto D (2002) Zircon trace element geochemistry: partitioning with garnet and the link between U-Pb ages and metamorphism. *Chemical Geology* **184**, 123–38.

Saha D, Sain A, Kundu P, Mazumder R and Kar R (2015) Tectonostratigraphic evolution of the Nellore Schist Belt, southern India, since the Neoarchean. In *Precambrian Basins of India: Stratigraphic and Tectonic Context* (eds R Mazumder and PG Eriksson), pp. 269–82. Geological Society of London, Memoirs 43.

Sain A and Saha D (2018) Structure and tectonics of a Mesoproterozoic ophiolite: insight from Kanigiri Ophiolite with a mélange zone, southern India. *Tectonophysics* **744**, 177–204.

Sain A, Saha D, Joy S, Jelsma H and Armstrong R (2017) New SHRIMP age and microstructures from a deformed A-type granite, Kanigiri, Southern India: constraining the hiatus between orogenic closure and post orogenic rifting. *Journal of Geology* **125**, 241–59.

Sarvothman H and Sesha Sai VV (2010) Global correlations of A-type granites and related rocks, their mineralization and significance in lithospheric evolution. In *Geological Survey of India International Geoscience Programme, Final Report IGCP-510*. Kolkata: Geological Survey of India, 2–14.

Sesha Sai VV (2009) Sheeted dykes in Kandra Ophiolite Complex, Nellore Schist Belt, Andhra Pradesh: vestiges of Precambrian oceanic crust. *Journal of the Geological Society of India* **74**, 509–14.

Sesha Sai VV (2013) Proterozoic granite magmatism along the Terrane Boundary Tectonic Zone to the east of Cuddapah Basin, Andhra Pradesh: petrotectonic implications for Precambrian crustal growth in Nellore Schist Belt of Eastern Dharwar Craton. *Journal of the Geological Society of India* **81**, 167–82.

Sesha Sai VV (2019) Proterozoic magnesian feldspathic magmatism in the Nallamalai fold belt, Southern India: petrogenesis of Vellaturu–Ipuru–Nakerikally (VIN) arc magmatic granites, Eastern Dharwar craton. *Journal of the Geological Society of India* **93**, 409–18.

Sesha Sai VV, Rama Rao G, Prasad GJS and Reddy VA (2013) Occurrence of rare titanium–niobium-rich astrophyllite in the Podili alkali granite pluton, Prakasam district, Andhra Pradesh, India. *Current Science* **104**, 1290–3.

Shand SJ (1943) *The Eruptive Rocks*, second edition, New York: John Wiley.

Simmat R and Raith MM (2008) U–Th–Pb monazite geochronometry of the Eastern Ghats Belt, India: timing and spatial disposition of poly-metamorphism. *Precambrian Research* **162**, 16–39.

Skjerlie KP and Johnston AD (1993) Fluid-absent melting behavior of an F-rich tonalitic gneiss at mid-crustal pressures: implications for the generation of anorogenic granites. *Journal of Petrology* **34**, 785–815.

Slaby E, Smigielski M and Kronz A (2011) Chaotic three-dimensional distribution of Ba, Rb and Sr in feldspar megacrysts grown in an open magma system. *Contributions to Mineralogy and Petrology* **162**, 909–21.

Smithson SB (1963) Granite studies. The Precambrian Fli granite: a geological and geophysical investigation. *Norges Geologiske Undersökelse Skrifter* **219**, 1–212.

Srinivasan KN and Roop Kumar D (1995) Geological mapping of Podili-Kanigiri section in northern part of Nellore Schist Belt, Prakasam district, AP. Progress Report of Geological Survey of India Field Season 1992–1993. GSI unpublished report.

Subramanyam KSV, Santosh M, Yang Q-Y, Zhang Z-m, Balaram V and Reddy UVB (2016) Mesoproterozoic island arc magmatism along the southeastern margin of the Indian Plate: evidence from geochemistry and zircon U-Pb ages of mafic plutonic complexes. *Journal of Asian Earth Sciences* **130**, 116–38.

Sun SS and McDonough WF (1989) Chemical and isotopic systematics of oceanic basalts: implications for mantle compositions and processes. In *Magmatism in the Ocean Basins* (eds AD Saunders and MJ Norry), pp. 313–45. Geological Society of London, Special Publication no. 42.

Turner SPJ, Foden D and Morrison RS (1992) Derivation of some A type magmas by fractionation of basaltic magma: an example from the Pathway Ridge, South Australia. *Lithos* **28**, 151–79.

Upadhyay D, Raith MM, Mezger K and Hammer Schmidt K (2006) Mesoproterozoic rift-related alkaline magmatism at Elchuru, Prakasam Alkaline Province, SE India. *Lithos* **89**, 447–77.

Vasudevan D and Rao TM (1976) The high grade schistose rocks of Nellore Schist Belt, Andhra Pradesh and their geologic evolution. *Indian Mineralogist* **16**, 43–7.

Vermeesh P (2018) IsoplotR: a free and open toolbox for geochronology. *Geoscience Frontiers* **9**, 1479–93.

Vernon RH (1984) Microgranitoid enclaves: globules of hybrid magma quenched in a plutonic environment. *Nature* **304**, 438–9.

Vernon RH, Etheridge MA and Wall VJ (1988) Shape and microstructure of microgranitoid enclaves: an indicator of magma mingling and flow. *Lithos* **22**, 1–11.

Vijaya Kumar K, Ernst WG, Leelanandam C, Wooden JL and Grove MJ (2010) First Paleoproterozoic ophiolite from Gondwana: geochronological–geochemical documentation of ancient oceanic crust from Kandra, SE India. *Tectonophysics* **487**, 22–32.

Vijaya Kumar K, Frost CD, Frost RB and Chamberlain KR (2007) The Chimakurti, Errakonda, and Uppalapadu plutons, Eastern Ghats Belt, India: an unusual association of tholeiitic and alkaline magmatism. *Lithos* **97**, 30–57.

Watson EB and Harrison TM (1983) Zircon saturation revisited: temperature and the composition effects in a variety of crustal magma types. *Earth and Planetary Science Letters* **64**, 295–304.

Whalen JB, Currie KL and Chappell BW (1987) A-type granites: geochemical characteristics, discrimination and petrogenesis. *Contributions to Mineralogy and Petrology* **36**, 1–22.

Whitney DL and Evans BW (2010) Abbreviations for names of rock-forming minerals. *American Mineralogist* **95**, 185–7.

Wickham SM, Albertz AD, Zanvilevich AN, Litvinovsky BA, Bindeman IN and Schauble A (1996) A stable isotope study of anorogenic magmatism in East Central Asia. *Journal of Petrology* **37**, 1063–95.

Yadav BS, Ahmad A, Kaulina T, Bayanova T and Bhutani R (2020) Origin of post-collisional A-type granites in the Mahakoshal Supracrustal Belt, Central Indian Tectonic Zone, India: zircon U-Pb ages and geochemical evidences. *Journal of Asian Earth Sciences.* doi: 10.1016/j. jseaes.2020.104247.

Yang JH, Wu FY, Chung SL, Chu MF and Wilde SA (2004) Multiple sources for the origin of granites: geochemical and Nd/Sr isotopic evidence from the Gudaoling granite and its mafic enclaves, northeast China. *Geochimica et Cosmochimica Acta* **68**, 4469–83.